Numerical calculation of gel electrophoretic mobility for "soft" spherical nanoparticles

Liji Le

Department of Chemical Engineering

McGill University, Montreal

June 2017

A thesis submitted to McGill University in partial fulfilment of the requirements for the degree of Master of Engineering

Preface

Contributions to the thesis are stated as follows:

Liji Le: (i) Performed all the calculations using the MPEK package developed by Reghan J. Hill; (ii) tested the MPEK package by direct comparisons with several theoretical calculations from earlier literature; (iii) interpreted literature gel electrophoresis data for "soft" nanoparticles using the MPEK package; (iv) wrote the thesis.

Reghan J. Hill (supervisor): (i) Developed the gel electrophoresis model for "soft" nanoparticles and programmed its solution in a computer program; (ii) edited the thesis draft; (iii) supervised the research.

Abstract

Gel electrophoresis is conventionally used for sorting and separating macromolecules. More recently it has been adopted for *nanoparticle* sorting and characterization. While the theoretical interpretation of free-solution (without gel) nanoparticle electrophoresis is well developed, models for interpreting nanoparticle gel electrophoresis are new. Hill (2016) recently developed a generalized electrokinetic model that accounts for polarization and relaxation effects to calculate the gel electrophoretic mobility of functionalized/soft spherical nanoparticles translating in charged and uncharged gels. The model captures hydrodynamic effects based on the Brinkman approximation for particles with arbitrary size, and includes pH charge regulation models. In this study, the model was applied to compare with independent calculations in the literature (including those undertaken using commercial finite-element software). It was also applied to interpret an experimental gel electrophoresis data for PEGylated nanoparticles with varying fraction of univalent PEG chains. The model accurately reproduced calculations in the literature, and extended the parameter space, now showing potential for quantitatively interpreting nanoparticle characterization and separation processes.

Abrégé

Le gel électrophorèse est conventionnellement utilisé pour organiser et séparer les macromolécules. Récemment, ils ont été adoptés pour l'organisation et la caractérisation des *nanoparticules*. Tandis que l'interprétation théorétique de solutions (sans gel) de nanoparticules électrophorèses est bien développée, des modèles pour l'interprétation des gels de nanoparticules électrophorèses sont nouveaux. Hill (2016) â récemment développé un modèle électrocinétique générale qui tient compte de la polarisation et les effets de relaxations pour calculer la mobilité du gel électrophorétique des nanoparticules sphériques fonctionnalisés en les traduisant en particules chargées et non-chargées. Le modèle englobe les effets hydrodynamiques basé sur l'approximation de Brinkman pour les particules de taille arbitraire, et inclut des modèles de régulation de la charge de pH. Dans cette étude, le modèle â été appliquée pour comparer avec des calculs indépendants dans la littérature (incluant ceux qui ont été effectuées en utilisant le logiciel commercial finite-element). Le modèle a aussi été appliqué pour interpréter des données expérimentales de gel électrophorèse pour PEGlayted nanoparticules avec une fraction variant d'univalent chaines de PEG. Le modèle a, avec précision, reproduit les calculs en littérature et élargit le paramètre d'espace, démontrant le potentiel pour quantitativement interpréter la caractérisation des nanoparticules et le procès de séparation.

Acknowledgments

My deepest gratitude goes first and foremost to my supervisor, Prof. Reghan J. Hill, Department of Chemical Engineering, for his constant guidance and encouragement. Without his support and instruction, the completion of this thesis would not be possible. Through these two years, what I learned is not only the knowledge about gel electrophoresis, but also the courage and confidence to overcome difficulties. I also would like to express my gratitude to my colleagues in Hill's research group, especially Mikhail Morunov and Cong Du, for their encouragement and assistance during these two years. I also sincerely thank my friends and fellow classmates. Besides, I gratefully acknowledge the financial support from Department of Chemical Engineering and my supervisor. Last, I thank my beloved parents for their unconditional love and great confidence in me through these years.

Contents

List of Figures

List of Tables

Chapter 1

Introduction

Nanotechnology is of great interest due to the unique properties and promising applications of nanoparticles. Nanoparticle surface modification, size, and shape are crucial for controlling the nanoparticle properties (Sosa et al., 2003; Win & Feng, 2005). Gel electrophoresis has recently been adopted for nanoparticle sorting and characterization. As compared to the well understood free-solution electrophoresis, the theoretical interpretation for nanoparticle gel electrophoresis is subject to present work. The presence of gel tremendously complicates the interpretation of nanoparticle electrophoretic mobility. The presence of a gel influences the nanoparticle mobility through hydrodynamic and steric effects. For nanoparticles that translating in dilute gels, the hydrodynamic effects are believed dominate. For larger particles translating in dense gels, the steric effect is expected to be the major influence on the nanoparticle electrophoretic mobility. An electrokinetic model that accounts for the gel hydrodynamics was first developed by Allison et al. (2007), using the Brinkman approximation to model the gel. Hill (2016) recently unified models of free-solution electrophoresis

for soft nanoparticles and models of gel electrophoresis for bare particles. This model accounts for polarization and relaxation effects, including pH charge regulation models for polyelectrolytes and charged gels. It calculates the gel electrophoretic mobility of functionalized/soft spherical nanoparticles translating in charged and uncharged gels.

This thesis focuses on applying the unified electrokinetic model to compare with independent calculations in the literature (including those undertaken using commercial finite-element software). After a thorough examination of this model, it was applied to interpret experimental gel electrophoresis data from Hanauer et al. (2007) for PEGylated nanoparticles with varying fraction of univalent PEG chains.

A literature review of the model development of free solution electrophoresis and gel electrophoresis for spherical particles is presented in Chapter 2. Chapter 3 briefly introduces the theory of the unified electrokinetic model developed by Hill (2016). Chapter 4 details the applications of this unified electrokinetic model for four different cases. Chapter 5 summarizes conclusions and makes recommendations for future work.

Chapter 2

Literature review

Gel electrophoresis, analogous to the electrophoresis in free-solution, is a widely used technique for separating macromolecules, such as DNA and proteins. In recent decades, the application of gel electrophoresis has been extended to nanoparticle separation and characterization (Sperling et al., 2006; Doane et al., 2010; Weidner et al., 2015). Zanchet et al. (2002) conducted a gel electrophoresis experiment that shows a successful separation of Au nanoparticles based on the amount of ssDNA attached to the nanoparticle surface (see fig. 2.1[1]). This study demonstrated that gel concentration has a significant influence on retarding the nanoparticle gel electrophoretic mobility. Hanauer et al. (2007) applied the gel electrophoresis technique to separate spherical nanoparticles according to their sizes and surface coatings. This study indicated that different functionalized PEGylated nanoparticles, such as SH-PEG-X molecules with X being -OCH3, -SH, -NH2, or -COOH, having significant

[1]Reprinted with permission from Zanchet et al. (2002). Copyright 2012 American Chemistry Society.

difference in electrophoretic mobility. However, theoretical interpretations of gel electrophoretic mobility of soft/functionalized nanoparticles are new. The development of electrophoretic mobility models for spherical particles are summarized as follows.

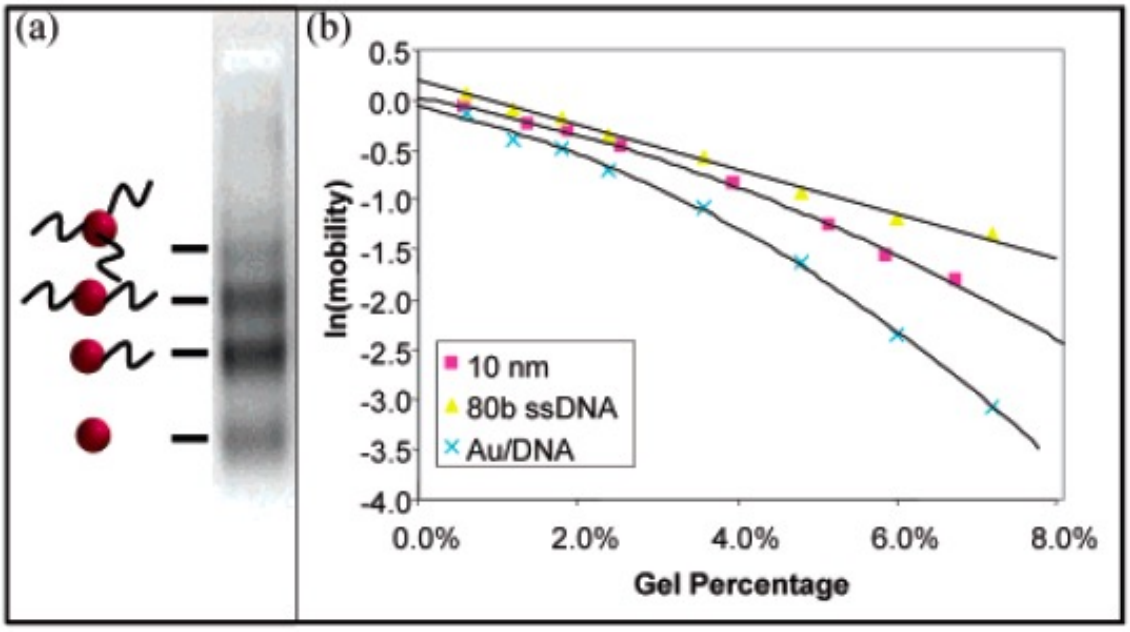

Figure 2.1: (a) Gel electrophoresis of gold nanoparticles. Each band corresponds to gold nanoparticles with well-defined numbers of ssDNA. (b) The relation between gel electrophoretic mobility and gel concentration (Zanchet et al., 2002).

Smoluchwski (1921) first developed an electrokinetic model to interpret the electrophoretic mobility of bare particles in free solution, whereas his formula is limited to the situation with low zeta-potential ($|\zeta| \ll k_B T/e$) and $\kappa a \gg 1$ (κ^{-1} is the Debye length of the particle double layer, a is the particle radius). Hückel (1924) then calculated the electrophoretic mobility for $\kappa a \ll 1$ and $|\zeta| \ll k_B T/e$. Henry (1931) generalized the model of free-solution electrophoresis of weakly charged bare spherical particles with arbitrary values of κa. These accomplishments did not account for the polarization (predominantly by electro-migration) and relaxation (by molecular diffu-

sion) effects, which have a significant effect when particles are highly charged (O'Brien & White, 1978). A brief description of polarization and relaxation effects is highlighted in fig. 2.2[2]. The figure shows that the particle couterions form a cloud that generates a local electric field that is opposite to the applied electric field.

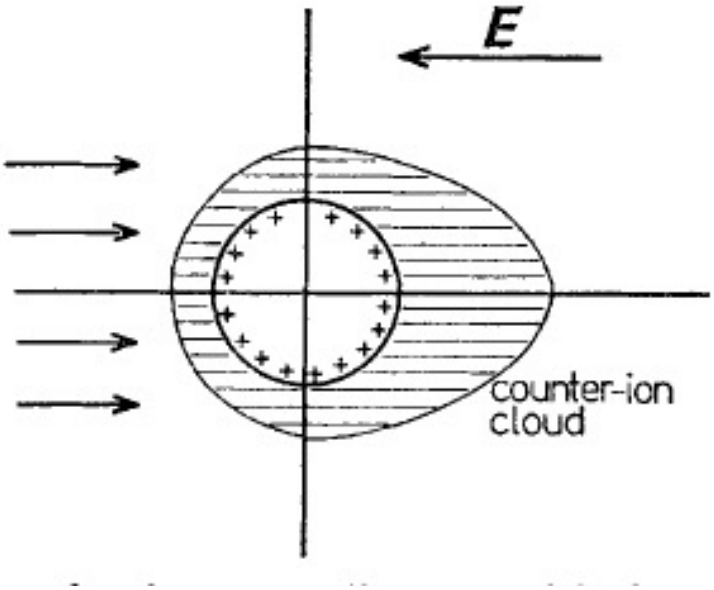

Figure 2.2: Sketch of the counterion cloud surrounding a positively charged colloidal particle translating in an electric field $\boldsymbol{E}$. The arrows indicate the direction of counterion electromigaration (O'Brien & White, 1978).

The first successful attempt to compute the polarization and relaxation effects is attributed to Overbeek Overbeek (1943), who derived analytical approximations (using perturbation methods) for particles having low-zeta potential $|\zeta| \ll k_B T/e$. Subsequent work by Wiersema et al. (1966), and O'Brien & White (1978) extended the theories to arbitrary values of κa using numerical methods, which solve the coupled nonlinear ordinary differential equations (Poisson, ion-conservation, fluid momentum,

[2]Reprinted with permission from O'Brien & White (1978). Copyright 1969 Royal Society of Chemistry.

and mass conservation equations). However, other complications arise from surface coatings, such as adsorbed or grafted polymers, which may be charged or uncharged. These modifications, though widely used (Couvreur, 1988; Greenwood & Kendall, 1999), are especially difficult to interpret by theory. Ohshima & Kondo (1989) generalized O'Brien's numerical solution of the standard electrokinetic model for bare particles to include a surface charge layer, presenting an approximate analytical solution without accounting for the polarization and relaxation effects. Hill & Saville (2005) developed a numerical theoretical solution for arbitrarily sized, soft spherical particles considering the polarization and relaxation effects. These generalized the electrophoresis model for "soft" particles in free solution for all particle sizes, and removed restrictions, such as a thin particle layer. Hill (2015a) recently proposed a pH-charge regulation model that advanced the model of free-solution electrophoresis for spherical particles to incorporate charge-regulated polyelectrolyte coatings.

Gel electrophoresis, compared to free-solution electrophoresis, has a gel medium in fluid. The gel network hinders particle motion according to many factors, such as particle size. A denser gel solution has a smaller pore size that enhances friction on the migrating particles. Similarly, larger particles tend to move slower, with a lower electrophoretic mobility. Apart from the size exclusion effect, charged gel can create an electroosmotic flow in the opposite direction to the movement of particles. Gel electrophoresis (e.g., agarose gels) has been shown to improve in macromolecular separations (Stellwagen, 2009). Hanauer et al. (2007) performed gel electrophoresis experiments to separate gold nanorods and spheres in gels with various gel concentrations, with the best separation efficiency achieved at 0.2 wt% agarose gel concentration.

As compared to free-solution electrophoresis, the calculation of gel electrophoretic mobility is even more difficult due to hydrodynamic and direct interactions between migrating particles and gel. Therefore, the electrokinetic models need to be modified to incorporate the gel effect. The hydrodynamic forces have been termed a long range interaction (Stigter, 2000), and the steric effects a short range effect. For large molecules, such as DNA (molecular size larger than the gel pore size), the short-range effects dominate, and reptation theories have been adopted to quantify gel electrophoresis (Calladine et al., 1991; Zimm & Levene, 1992). For particles that are small (particle radius smaller than the gel pore size), electrokinetic models have been adopted to model the electrophoretic mobility of particles based on the Brinkman approximation of a gel (Brinkman, 1949; Debye & Bueche, 1948; Felderhof & Deutch, 1975; Allison et al., 2007).

An electrokinetic model to interpret nanoparticle gel electrophoresis was first developed by Allison et al. (2007). Inspired by the successful application of the Brinkman effective model for describing the electrophoretic relaxation of a single, initially stretched DNA molecule in a gel support medium (Stigter, 2000) as well as in describing the diffusion of particles in a gel (Pluen et al., 1999), Allison et al. (2007) proposed a model to study the problem of electrophoresis of spheres in a gel support medium. They successfully derived an analytical formula for the electrophoretic mobility of a weakly charged bare sphere in an uncharged gel, and addressed the nonlinear electrostatics and ion-concentration perturbation effects numerically when particles are highly charged. Allison et al. (2007) also proposed a model to account for the gel steric effects in dilute gels. Fixed charge on the hydrogel couple with the

mobile countercharge to influence the particle diffuse layer, imposing an additional electro-osmotic disturbance to the migrating particle. Hanauer et al. (2007) conducted gel electrophoresis experiments, discovering an electro-osmotic flow in agarose gels (uncharged gel). This phenomenon indicates that even for uncharged gels, which have no ion dissociation, mobile countercharge still exists. Hanauer et al. (2007) assumed that the electro-osmotic flow driven by a gel could be added to the nanoparticle gel electrophoretic velocity to furnish the intrinsic gel electrophoretic mobility, which neglects the nanoparticle disturbance to the electro-osmotic velocity.

Electrophoresis in charged gels is much more difficult to interpret. Doane et al. (2010) developed a closed-form solution for the gel electrophoresis of a weakly charged, impenetrable sphere bearing a thin polymer coatings. By fitting the gel electrophoresis data of PEGylated Au NPs for several agarose gel concentrations, this model elucidates how the charges on gel influence the nanoparticle mobility. Adopting the gel Brinkman model, Hsu et al. (2013) stuided the gel electrophoresis of a charge-regulated bi-functional particle containing both acidic and basic functional groups on its surface. They proposed a charge-regulation model to study surface dissociation/association reactions. Motivated by studies of charge-regulated interfaces (Healy & White, 1978; Chen et al., 2014), Hill (2015b) proposed a charge-regulation model to study charge density perturbations in hydrogels. He concluded that charge density perturbations in hydrogels are mainly produced by the equilibrium electrostatic potential induced by the particle surface charge (termed the primary immobile charge density perturbation), while the charge density perturbations generated by the external forces (termed the secondary immobile charge-density) have a negligible effect on

the particle mobility. Similar to free-solution electrokinetic models for soft particles, extensive studies have been carried out to study the problem of gel electrophoresis for spherical polymer coated particles. These models are still subject to the Debye-Hückel approximation (relaxation effects ignored) (Li et al., 2014; Allison et al., 2014). Allison et al. (2016) generalized the problem of gel electrophoretic mobility to include the relaxation effects for highly charged nanoparticles, including grafted polymer or polyelectrolytes–termed "soft" nanoparticles, also addressing the effect of hydrogel charge. However, this model is limited to polymer coatings with uniform charge density and Brinkman screening length, which is impractical for many real applications.

Chapter 3

Theory

Hill (2016) recently developed a generalized electrokinetic model that accounts for polarization and relaxation effects to calculate the gel electrophoretic mobility of functionalized/soft spherical nanoparticles translating in charged and uncharged gels. The model captures hydrodynamic effects based on the Brinkman approximation for particles with arbitrary size, and includes pH-charge regulation models. This model unified electrokinetic models developed in two earlier studies (Hill, 2015a,b). Polymer coatings and the hydrogel are both treated as Brinkman porous media. As illustrated in fig. 3.1, particles translate with a velocity $\boldsymbol{V}$ in a constant external electric field $\boldsymbol{E}$. An electroosmotic fluid velocity $\boldsymbol{u}$ is created in the opposite direction to the particle translation. The polymer coatings and hydrogels may be polyelectrolytes. The charges on the polyelectrolytes could be acidic, basic, or amphoteric, all of which are modeled by pH-charge regulation model. For this electrokinetic model, the particles are dilute and, therefore, particle interactions are neglected.

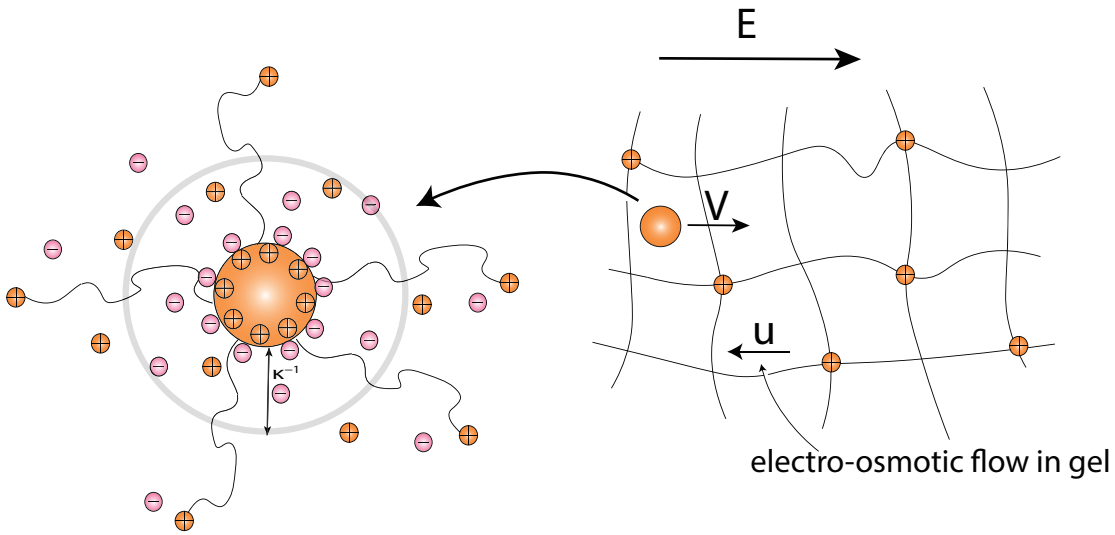

Figure 3.1: Sketch of a nanoparticle translating in gels under a constant electric field $\boldsymbol{E}$. $\boldsymbol{V}$ is the particle velocity, and $\boldsymbol{u}$ is the fluid velocity in the gel.

The following equations combine the governing equations from the models of gel electrophoresis for bare particles (Hill, 2015b) and models of free-solution electrophoresis for "soft" particles (Hill, 2015a), comprising the Poisson, ion-conservation, fluid momentum, and mass conservation equations to model the motion of the particles in gel solution under a weak and constant electric field $\boldsymbol{E}$:

$$-\epsilon_o\epsilon_s\nabla^2\psi = \rho_m + \rho_{f,1} + \rho_{f,2} \tag{3.1}$$

$$0 = -\boldsymbol{\nabla}\cdot\left(n_i\boldsymbol{u} - D_i\boldsymbol{\nabla}n_i - z_i e\frac{D_i}{k_BT}n_i\boldsymbol{\nabla}\psi\right) \quad (i = 1\ldots N) \tag{3.2}$$

$$0 = \eta\nabla^2\boldsymbol{u} - \boldsymbol{\nabla}p - \frac{\eta}{\ell_1^2}(\boldsymbol{u}-\boldsymbol{V}) - \frac{\eta}{\ell_2^2}\boldsymbol{u} - \rho_m\boldsymbol{\nabla}\psi \tag{3.3}$$

$$0 = \boldsymbol{\nabla}\cdot\boldsymbol{u} \tag{3.4}$$

with

$$\rho_m = \sum_{j=1}^{N} z_j e n_j \tag{3.5}$$

Here, ψ is the electrostatic potential, ϵ_s, η are the solvent relative permittivity and viscosity, $\boldsymbol{u}$ and p are the fluid velocity and pressure. Ion concentrations in the electrolyte are denoted by n_i, and the subscript i represents the i^{th} ion species, each of which has its distinct charge $z_i e$ and mobility $D_j/(k_B T)$, where D_j is a diffusion coefficient, and $k_B T$ is the thermal energy. The total mobile charge density ρ_m is the sum of the ion concentrations times its charge. Further, $\rho_{f,1}$ and $\rho_{f,2}$ are the fixed charge densities on the polyelectrolyte and hydrogels, respectively. The Brinkman screening lengths ℓ_1 (coatings) and ℓ_2 (hydrogel) are related to the number density of polymer segments n_s. It is assumed that the hydrogels are uniformly distributed, so, a constant Brinkman screening length ℓ_2 and fixed charge density $\rho_{f,2}$ are used in the electrokinetic model. For polymer coatings, the Brinkman screening length ℓ_1 and fixed charged density $\rho_{f,1}$ are likely to have a non-uniform distribution around the particle core.

The above equations are solved with the procedures set out in earlier studies (Hill, 2015a,b) by expressing the variables as the sum of the equilibrium solutions and their perturbations.

3.1 Equilibrium solution

The equilibrium state, identified with the superscript 0, corresponds to a stationary particle, polyelectrolyte layer, and electrolyte in the absence of any external forcing. The equations are then reduced to

$$-\epsilon_p\epsilon_s\nabla^2\psi^0 = \sum_{j=1}^{N} z_j e n_j^0 + \rho_{f,1}^0 + \rho_{f,2}^0 \tag{3.6}$$

$$0 = -\boldsymbol{\nabla}\cdot\left(-D_i\boldsymbol{\nabla}n_i^0 - z_i e\frac{D_i}{k_B T}n_i^0\boldsymbol{\nabla}\psi^0\right) \quad (i = 1\ldots N) \tag{3.7}$$

$$0 = -\boldsymbol{\nabla}p^0 - \sum_{j=1}^{N} z_j e n_j^0\boldsymbol{\nabla}\psi^0 \tag{3.8}$$

3.2 Perturbations

The following equations are extracted directly from the theories in Hill (2015a). Linear perturbations can reasonably approximate the external forcing when the applied electric field is weak. Since the model is truncated to linear order in these perturbations, linearity and symmetry considerations demand solutions that have following forms:

$$\boldsymbol{u} = \boldsymbol{\nabla}\times\boldsymbol{\Phi} + \boldsymbol{U} \text{ with } \boldsymbol{\Phi} = \hat{f}(r)\boldsymbol{X}\times\boldsymbol{e}_r, \tag{3.9}$$

$$\psi = \psi^0(r) + \psi' \ , \ n_j = n_j^0(r) + n_j' \ , \ p = p^0(r) + p', \tag{3.10}$$

where

$$\psi' = \hat{\psi}(r)\boldsymbol{X}\cdot\boldsymbol{e}_r - \boldsymbol{E}\cdot\boldsymbol{r}\ ,\ n_i' = \hat{n}_i(r)\boldsymbol{X}\cdot\boldsymbol{e}_r\ ,\ p' = \hat{p}(r)\boldsymbol{X}\cdot\boldsymbol{e}_r + \boldsymbol{P}\cdot\boldsymbol{r} \tag{3.11}$$

Here, $\boldsymbol{X} = X\boldsymbol{e}_z$ denotes the vector (directed along the z-axis) that drives the perturbations: either the applied electric field vector $\boldsymbol{E} = E\boldsymbol{e}_z$ or particle velocity $\boldsymbol{V} = V\boldsymbol{e}_z$. Note that $P = 0$ is the far-filed pressure gradient, and $\boldsymbol{U} = U\boldsymbol{e}_z$ is the far-field fluid velocity; moreover, $\boldsymbol{r} = r\boldsymbol{e}_r$ is the position vector, where $\boldsymbol{e}_r$ is the radial unit vector.

In the linear approximation, the perturbations satisfy:

$$-\epsilon_o\epsilon_s\nabla^2\psi' = \rho_m' + \rho_{f,1}' + \rho_{f,2}' \tag{3.12}$$

$$0 = -\boldsymbol{\nabla}\cdot\left(n_i^0\boldsymbol{u} - D_i\boldsymbol{\nabla}n_i' - z_ie\frac{D_i}{k_BT}n_i'\boldsymbol{\nabla}\psi^0 - z_ie\frac{D_i}{k_BT}n_i^0\boldsymbol{\nabla}\psi'\right)\quad (i = 1\ldots N) \tag{3.13}$$

$$0 = \eta\nabla^2\boldsymbol{u} - \boldsymbol{\nabla}p' - \frac{\eta}{\ell_1^2}(\boldsymbol{u}-\boldsymbol{V}) - \frac{\eta}{\ell_2^2}\boldsymbol{u} - \rho_m'\boldsymbol{\nabla}\psi^0 - \rho_m^0\boldsymbol{\nabla}\psi' \tag{3.14}$$

$$0 = \boldsymbol{\nabla}\cdot\boldsymbol{u} \tag{3.15}$$

Taking the curl of the momentum equation (to eliminate the pressure) and writing the perturbation equations in terms of the radial perturbation functions (hatted variables) furnishes the linear ordinary differential system[1]:

[1]These equations are derived based on two earlier studies (Hill, 2015a,b). I have independently

$$-\epsilon_o\epsilon_s\mathscr{L}_1\hat{\psi} = \sum_{j=1}^{N} z_j e\hat{n}_j + \sum_{j=1}^{N}\hat{\rho}_{f,j} \tag{3.16}$$

$$\begin{aligned} 0 = n^0_{i,r}(2r^{-1}\hat{f}X + U - V) - D_i\mathscr{L}_1\hat{n}_i X - z_i e\frac{D_i}{k_B T}(\hat{n}_{i,r}\psi^0_r + \hat{n}_i\mathscr{L}_0\psi^0)X... \\ -z_i e\frac{D_i}{k_B T}[(\hat{\psi}_r X - E)n^0_{i,r} + n^0_i\mathscr{L}_1\hat{\psi}X] \quad (i = 1...N) \end{aligned} \tag{3.17}$$

$$\begin{aligned} 0 = -\eta\mathscr{L}_2\hat{f}_{rr}X + \frac{\eta}{\ell_1^2}\mathscr{L}_1\hat{f}X + \eta(\ell_1^{-2})_r(\hat{f}_r + r^{-1}\hat{f})X + \eta(\ell_1^{-2})_r U... \\ +\frac{\eta}{\ell_2^2}\mathscr{L}_1\hat{f}X - \sum_{j=1}^{N} z_j e\hat{n}_j r^{-1}\psi^0_r X + \sum_{j=1}^{N} z_j e n^0_{j,r} r^{-1}(\hat{\psi}X - rE), \end{aligned} \tag{3.18}$$

where subscripts r denote radial differentiation, and $\mathscr{L}_0(\cdot) = (\cdot)_{rr} + 2r^{-1}(\cdot)_r$, $\mathscr{L}_1(\cdot) = (\cdot)_{rr} + 2r^{-1}(\cdot)_r - 2r^{-2}(\cdot)$ and $\mathscr{L}_2(\cdot) = (\cdot)_{rr} + 4r^{-1}(\cdot)_r - 4r^{-2}(\cdot)$.

Forces acting on the "soft" nanoparticle can be evaluated by superposition of the so-called V and E-problems employed by Hill (2015a). Balancing the hydrodynamic drag forces and the Coulomb forces furnishes the electrophoretic mobility. These calculations are undertaken by the MPEK package and many results are readily available from Hill (2016).

verified them. The equation similar to Eqn. 3.18 in Hill (2015a) has a typo: $\frac{\eta}{\ell_1^2}\mathscr{L}_1\hat{f}$ should read $\frac{\eta}{\ell_1^2}\mathscr{L}_1\hat{f}X$.

Chapter 4

Results and discussion

4.1 Charge regulated, bi-functional particles in uncharged gels

The present model is examined by considering a charge regulated, bi-functional particle in uncharged gels, and the results are compared with Hsu et al. (2013). The particle has both acidic and basic functional groups on its surface. The dissociation/association reaction of these two functional groups can be expressed as AH $\longleftrightarrow$ A^- + H^+, and BH^+ $\longleftrightarrow$ B + H^+, respectively. $K_A = [A^-][H^+]/[AH]$, $K_B = [B][H^+]/[BH^+]$ are the coresponding equilibrium constants. In Hsu et al. (2013)'s simulation, AH and B are specifically chosen as glutamic acid with pK_A = 4.1 and lysine with pK_B = 10.5 (Smejtek et al., 2010)[1]. N_{AH} and N_B denote the number of functional groups AH and B on the particle surface, respectively; $\tau = N_{AH}/N_B$

[1]The values pK_A = 10.5, and pK_B = 4.1 stated in Hsu et al. (2013) are mixed (Smejtek et al., 2010).

denotes the ratio of those two groups. There is an error in definition of the dimensionless density of the functional groups, which is corrected as $\xi = (n^*_{f,A} e^2 a/\epsilon k_B T)$, with ϵ and e being the solvent permittivity and fundamental charge, respectively; $n^*_{f,A} = N_{AH}/4\pi a^2$ is the biding-site density of acid groups on particle surface, with a similar definition for basic groups. Hsu et al. (2013) have erroneously mixed the variables $n_{f,A}$ and N_{AH} in the definition of the dimensionless density of the functional group. The gel is uncharged, and modeled as a Brinkman porous medium with $\ell_2 = a$, where a is the particle radius.

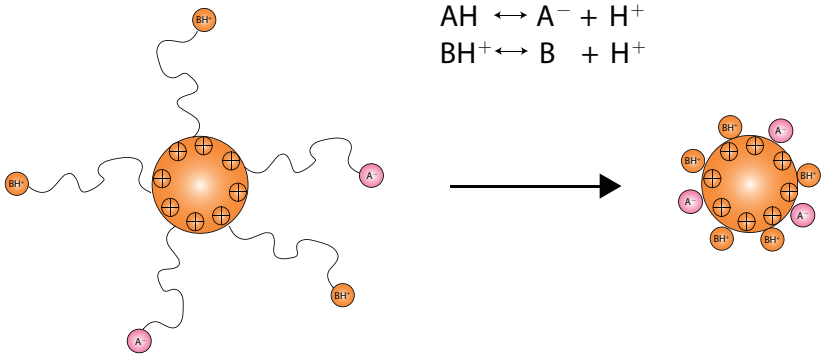

Figure 4.1: Left is a "soft" particle with charge regulated bi-functional polyelectrolyte; right is a charge-regulated bi-functional bare particle.

.

The model could be adopted to solve the present problem with appropriate settings of the corona geometry parameters. The bare particle with bi-functional groups on its surface is analogous to the particle with an infinitesimally thin polyelectrolyte layer, as shown in fig. 4.1.

Following Hill et al. (2015), the number densities of polymer segments and of fixed charge for the bi-functional groups are specified using Gaussian functions:

$$n_s(r) = n_{s,0} e^{-(r-L_1-a)^2/\delta_1^2} \tag{4.1}$$

and

$$n_f^*(r) = n_{f,0} e^{-(r-L_2-a)^2/\delta_2^2}, \tag{4.2}$$

where

$$N_s N_a = \int_a^\infty n_s(r) 4\pi r^2 \mathrm{d}r = 4\pi a^3 n_{s,0} f(\delta_1/a, L_1/a) \tag{4.3}$$

and

$$N_c = \int_a^\infty n_f^*(r) 4\pi r^2 \mathrm{d}r = 4\pi a^3 n_{f,0} f(\delta_2/a, L_2/a) \tag{4.4}$$

with

$$f(x,y) = x^2 e^{-(y/x)^2}(y+2)/2 + x(1/2)\sqrt{\pi}(y^2+2y+x^2/2+1)[1+\mathrm{erf}(y/x)].$$

Here, N_c denotes the number of functional groups, for acid groups AH: $N_c = N_{AH}$, for basic groups B: $N_c = N_B$, N_a is the aggregation number of ligands with N_s the number of segments in a chain. n_s is the corona segment density, n_f^* is the binding-site density of the bi-functional groups, expressed as $n_{f,A}^* = [\mathrm{A}^-] + [\mathrm{AH}]$, $n_{f,B}^* = [\mathrm{B}] + [\mathrm{BH}^+]$, where subscript A, B represent the acid and basic groups respectively. ρ_f^* is the fixed charge density determined by the dissociation of H^+ from AH, and association of H^+ with B. Fig. 4.2 illustrates the distribution of the biding-site density of functional groups, and number density of polymer segments.

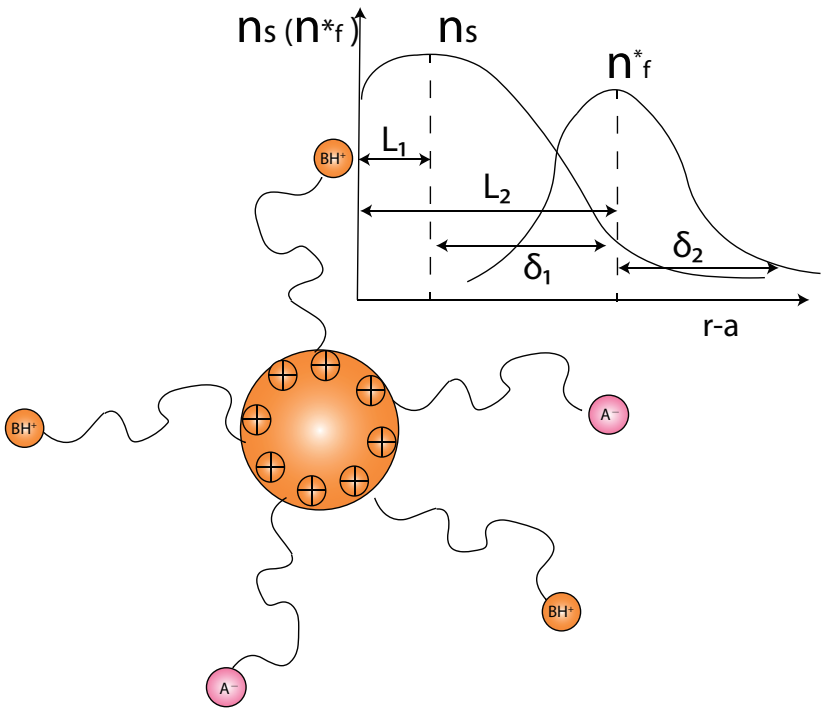

Figure 4.2: Gaussian distribution of biding-site density of bi-functional groups n_f^*, and number density of polymer segments n_s.

.

The fixed charge density ρ_f^* is related to the biding-site density of acid and basic groups. Following Hsu et al. (2013),

$$[\mathrm{A}^-] = \frac{[\mathrm{AH}] + [\mathrm{A}^-]}{1 + \frac{[\mathrm{H}^+]_0}{K_A}\exp(-e\psi_e/k_BT)}$$

and

$$[\mathrm{BH}^+] = \frac{([\mathrm{B}] + [\mathrm{BH}^+])\frac{[\mathrm{H}^+]_0}{K_B}\exp(-e\psi_e/k_BT)}{1 + \frac{[\mathrm{H}^+]_0}{K_A}\exp(-e\psi_e/k_BT)},$$

so the fixed charge density ρ_f^* associated with H^+ mobile ion can be written

$$\rho_f^* = e\frac{n_{f,A}^*}{1 + \frac{[\mathrm{H}^+]_0}{K_A}\exp(-e\psi_e/k_BT)} - e\frac{n_{f,B}^*\frac{[\mathrm{H}^+]_0}{K_B}\exp(-e\psi_e/k_BT)}{1 + \frac{[\mathrm{H}^+]_0}{K_A}\exp(-e\psi_e/k_BT)}.$$

In the present problem, corona parameters $L_1 = 0$ represent the maximum polymer segment density at the particle surface. The nominal corona thickness could be mimicked by varying δ_1; the polyelectrolyte is normally assumed as being terminally charged (Hill, 2015a; Hill et al., 2015), e.g., $L_2 = \delta_1$ as shown in fig. 4.1. In the present application, $L_2 = 0$ is used to model the particle charge-regulated surface with $\delta_2 = \delta_1$. By taking limit of the nominal thickness to an infinitesimal value (relative to the particle radius), the generalized electrokinetic model could be applied to the present problem.

Fig. 4.3 shows that particles with polyelectrolyte layer of $\delta_1/a = 0.005$ and $\delta_1/a = 0.001$ have the same surface potential in the range of κa from 0.1 to 20. However, the particle with polyelectrolyte layer of $\delta_1/a = 0.01$ has a lower surface potential at large κa. The screening effect plays a key role in attenuating the surface potential at high ionic strength where the Debye length κ^{-1} is comparable to the corona thickness. It suggests that polyelectrolytes with $\delta/a = 0.01$ are not sufficiently thin to model the present problem. Surface charge densities for soft (thin polyelectrolyte-coating) spheres with $\delta_1/a = 0.01$, $\delta_1/a = 0.005$, $\delta_1/a = 0.001$ are shown in fig. 4.4. Particles with corona thickness of $\delta_1/a = 0.01$, $\delta_1/a = 0.005$ again converge to the same surface charge density in the above range of κa. In this study, surface charge density is directly converted from the net particle valence Z, which is conveniently ascertained by numerically evaluating the integral (Hill et al., 2003b):

$$Z = \sum_{j=1}^{N} n_j^{\infty} z_j \int_a^{\infty} (e^{-z_j e\psi^0/k_B T} - 1) 4\pi r^2 \mathrm{d}r,$$

and, if the corona is thin enough, then

$$\sigma_p^* \approx \frac{ae}{\epsilon k_B T} \frac{Ze}{4\pi a^2}.$$

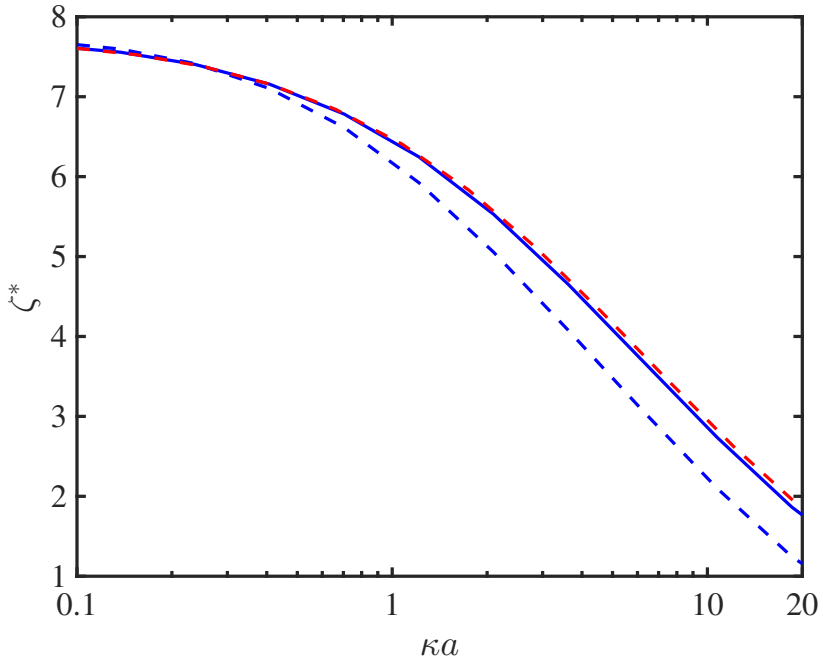

Figure 4.3: Scaled surface potential ζ^* for soft (thin polyelectrolyte-coating) spheres ($a = 5$ nm) translating in uncharged gels. The blue dashed line, blue solid line and red dashed line are for particles of corona thickness $\delta_1/a = 0.01$, $\delta_1/a = 0.005$, $\delta_1/a = 0.001$, respectively. Parameters are the same as Hsu et al. (2013): pH = 7, $\tau = 0.5$, $\mathrm{p}K_\mathrm{A} = 4.1$, $\mathrm{p}K_\mathrm{B} = 10.5$, and gel Brinkman screening length $\ell_2 = a$.

.

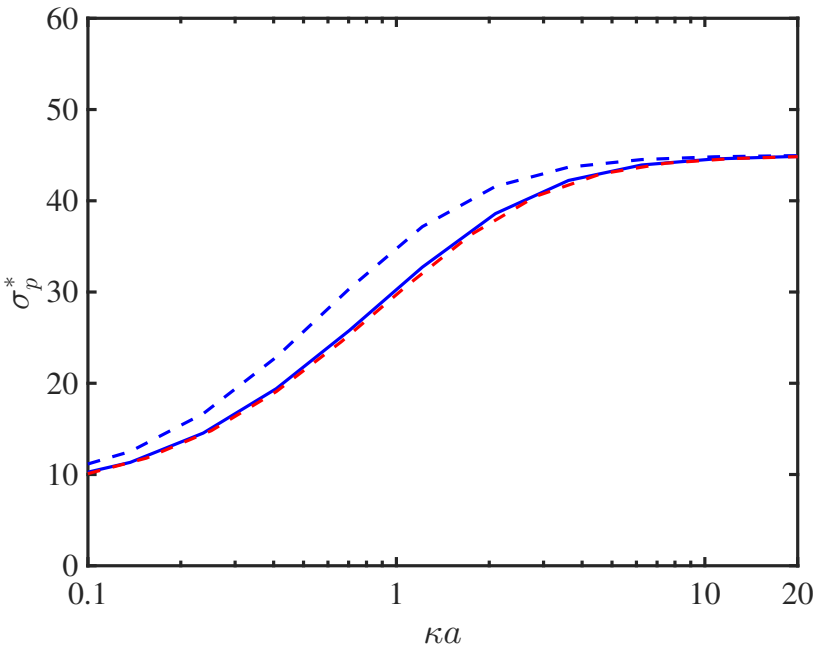

Figure 4.4: Scaled surface charge density σ_p^* for soft (thin polyelectrolyte-coating) spheres ($a = 5$ nm) translating in uncharged gels. The blue dashed line, blue solid line and red dashed line are for particles of corona thickness $\delta_1/a = 0.01$, $\delta_1/a = 0.005$, $\delta_1/a = 0.001$, respectively. Parameters are the same as Hsu et al. (2013): pH = 7, $\tau = 0.5$, p$K_{\rm A} = 4.1$, p$K_{\rm B} = 10.5$, and $\ell_2 = a$.

.

A test of the parameter ξ on the influence of the charge density and surface potential is conducted and the results are compared with Hsu et al. (2013). Figs. 4.5 and 4.6 show that the results modeled by soft (thin polyelectrolyte-coating with $\delta_1/a = 0.005$) particles with various values of ξ are all in excellent agreement with Hsu et al. (2013). These results again reveal that the nominal corona thickness ($\delta_1/a = 0.005$) is thin enough to model the present problem. Cautiously, a polyelectrolyte-coating with $\delta_1/a = 0.001$ is used in the following calculations.

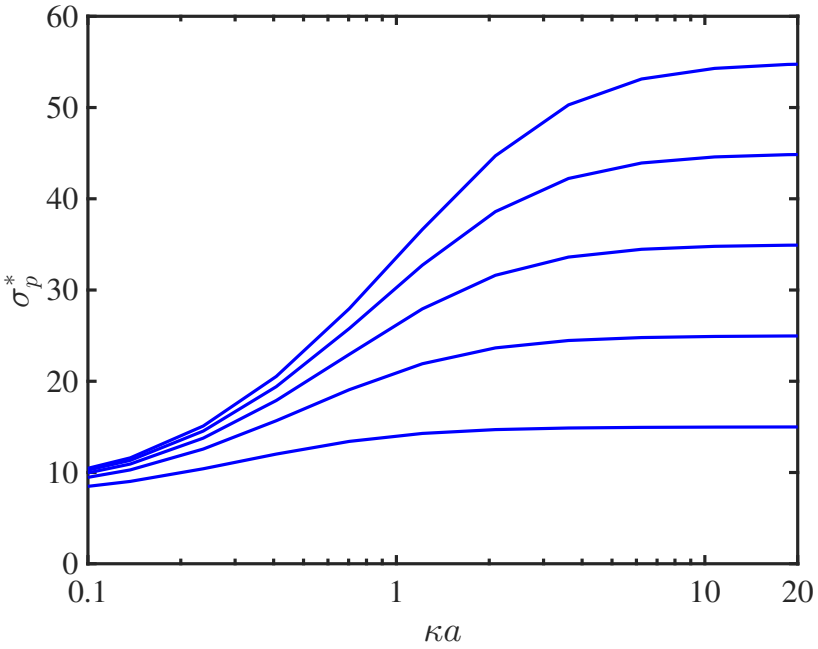

Figure 4.5: Model validation by reproduction of fig. 4 of Hsu et al. (2013) for soft (thin polyelectrolyte-coating with $\delta_1/a = 0.005$) spheres ($a = 5$ nm) dispersed in an uncharged gel. Scaled surface charge density σ_p^* as a function of κa for various values of $\xi = 15, 25, 35, 45, 55$ (increasing upward). Parameters are the same as Hsu et al. (2013): pH $= 7$, $\tau = 0.5$, p$K_{\rm A} = 4.1$, p$K_{\rm B} = 10.5$, and $\ell_2 = a$.

.

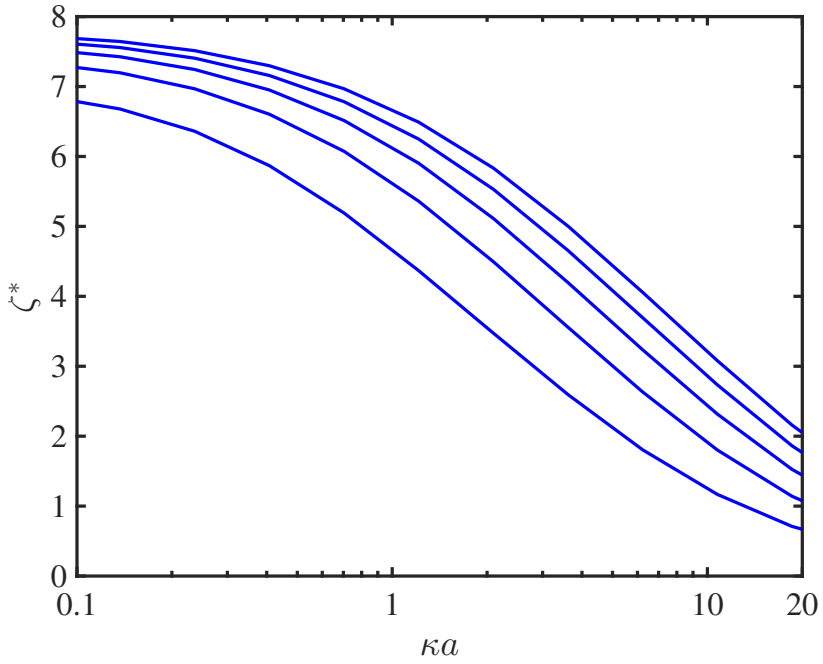

Figure 4.6: Model validation by reproduction of fig. 4 of Hsu et al. (2013) for soft (thin polyelectrolyte-coating with $\delta/a = 0.005$) spheres ($a = 5$ nm) dispersed in an uncharged gel. Scaled surface potential ζ^* as a function of κa for various values of $\xi = 15, 25, 35, 45, 55$ (increasing upward). Parameters are the same as Hsu et al. (2013): pH = 7, $\tau = 0.5$, $\mathrm{pK_A} = 4.1$, $\mathrm{pK_B} = 10.5$, and $a = \ell_2$.

.

Finally, the generalized electrokinetic model is tested by calculating the electrophoretic mobility under various pH over a wide range of κa. The scaling factor applied to the dimensionless mobility from the MPEK package includes a factor of 3/2:

$$M^* = \frac{3\eta e}{2\epsilon k_B T} M. \tag{4.5}$$

To make it consistent with the dimensionless mobility[2] in Hsu et al. (2013), a factor of 2/3 is needed to multiply the dimensionless mobility from the MPEK package. The generalized electrokinetic model successfully reproduces figs. 7 and 8 in Hsu et al.

[2] $M^* = \frac{\eta e}{\epsilon k_B T} M$ in Hsu et al. (2013).

(2013), as presented in fig. 4.7. Meanwhile, the model can extend the applicability of the current problem to a broader range of ionic strengths. From the figure, a lower limit on κa is realized for each of the four cases pH = 7, 8, 8.5, 9. The lower limit on κa is restricted by the minimum ion concentration reached for each cases. Fig. 4.7 d shows that the Brinkman factor approaches a specific constant in a lower limit and higher limit of κa. This limit is calculated by the Brinkman formula (Brinkman, 1949; Stigter, 2000):

$$F_B = 1 + \frac{a}{\ell_2} + \frac{(a/\ell_2)^2}{9}, \tag{4.6}$$

which is originally applicable to uncharged spheres translating in an uncharged Brinkman medium. Hill & Li (2013) recently showed that the Brinkman formula is also applicable to charged spheres translating in Brinkman medium at sufficiently low and high ionic strengths. For the present case, the drag coefficient F is expected to asymptote to 2.111. More interestingly, the mobility at the vanishing ionic strength ($\kappa a \to 0$) can be independently verified by the Hückel approximation (Hill, 2015b):

$$M = \frac{Ze}{6\pi\eta a_h} (\kappa a \to 0). \tag{4.7}$$

This is achieved by balancing the Coulomb force ZeE with the hydrodynamic drag $-6\pi\eta a_h V$. Here, hydrodynamic radius a_h is related to the drag coefficient $F = a_h/a$. In the limit of low ionic strength ($\kappa a \to 0$), the relaxation effects vanish, and $a_h = F_B a$. The red dashed line in fig. 4.7 a comes from applying Eqns. 4.6 and 4.7. It indicates that Hückel approximation is in excellent agreement with the model calculations.

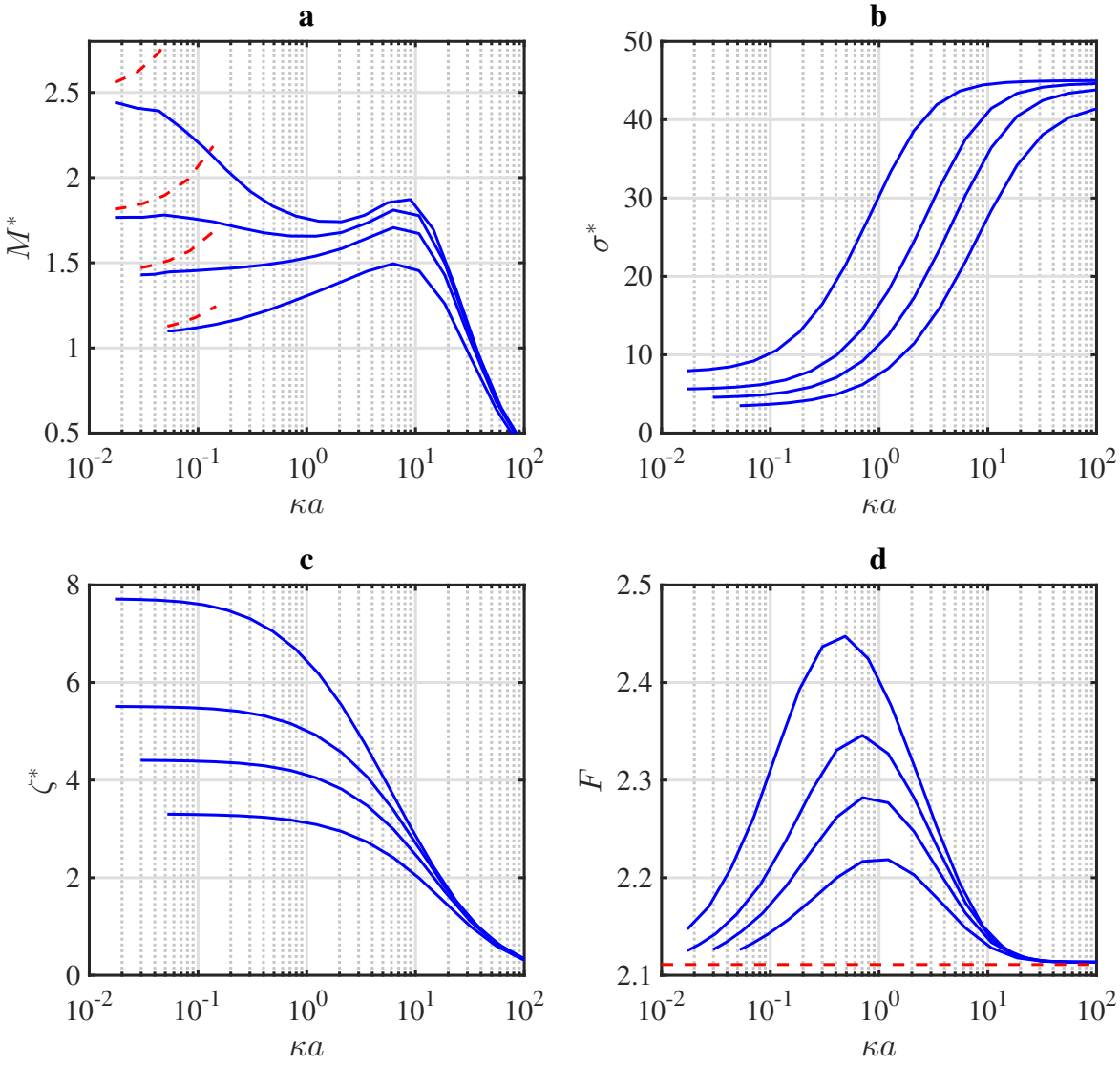

Figure 4.7: Model validation by reproduction of figs. 7 and 8 of Hsu et al. (2013) with soft (thin polyelectrolyte-coating with $\delta_1/a = 0.001$) spheres ($a = 5$ nm) dispersed in an uncharged gel with bulk pH= 7, 8, 8.5, 9, from uppermost to lowermost. Other parameters: $\tau = 0.5$, p$K_A = 4.1$, p$K_B = 10.5$, and $\ell_2 = a$. (a) Scaled electrophoretic mobility versus κa. Dashed lines are the Hückel mobilities, $M = Ze/(6\pi\eta aF)$ when $(\kappa a \to 0)$; (b) Scaled surface charge density versus κa; (c) Scaled surface potential versus κa; (d) Drag coefficient F versus κa. Dashed line is the Brinkman formula.

.

4.2 Highly charged particles in uncharged gels

In this section, following Allison et al. (2007), the electrokinetic model is applied to calculate the electrophoretic mobility of gold nanoparticles translating in uncharged gels. When interpreting the electrophoretic mobility of highly charged particles, it is necessary to account for the relaxation effects (distortion of the charge distribution due to the imposition of an external electric field) (O'Brien & White, 1978). Here, charged particles with a range of surface potentials are used to study the influence of the gel on the particle relaxation effects. The gel material is modeled as a continuous effective medium with gel screening parameter λ (reciprocal of the Brinkman screening length ℓ_2). This medium comprises solvent (solvent viscosity $\eta = 0.0089$ Pa s), multiple mobile ions (K^+, Cl^-, H^+, OH^-).

Following Allison et al. (2007), the same dimensionless variables λ/κ are considered for particles with different surface potential $Y = e\zeta/k_BT$ over a wide range of κa. It is assumed the particle core has a uniform electrostatic surface potential ζ, and that there is no electric or flow induced change in the electrostatic surface potential when a weak external electric field is applied.

Results are presented in figs.[3] 4.8, 4.9, and 4.10, which correspond to particles with surface potentials $Y = 1$, 3, and 5, respectively. To eliminate the influence of charge on the magnitude of the electrophoretic mobility, all those three figures are plotted with M^*/Y over a wide range of κa for different gel parameters λ/κ. Similar trends with the results of Allison et al. (2007) are found, with slight differences no-

[3]All data presented in Allison et al. (2007) have evidently been erroneously shifted one unit to the right along the x-axis.

ticed. However, Allison et al. (2007) addressed that their calculations are in excellent agreement with early studies in the absence of gel. Therefore, we calculated the free solution electrophoretic mobilities for particles with various surface potentials using the generalized electrokinetic model, and the results are compared with the reference Allison cited (Wiersema et al., 1966). Fig. 4.12 shows the electrophoretic mobilities of charged particles with various surface potentials $Y = 1, 2, 3, 4, 5$ translating in a free solution over a wide range of κa. We found that our calculation is accurate for particles with all surface potentials over the whole range of κa.

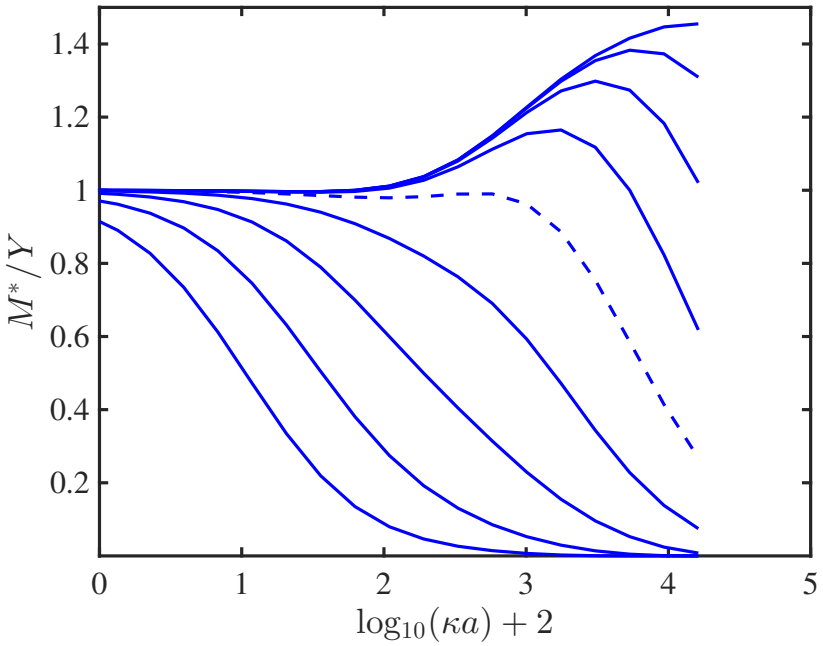

Figure 4.8: Model validation by reproduction of fig. 2 of Allison et al. (2007). Scaled mobility over particle surface potential versus $\log_{10}(\kappa a)+2$ with relaxation effects and $Y = 1$ for charged particles in uncharged gels with Brinkman screening parameter λ/κ = 0, 0.01, 0.027, 0.072, 0.193, 0.519, 1.389, 3.727, 10 (decreasing downward). Dashed line is for $\lambda/\kappa = 0.193$.

.

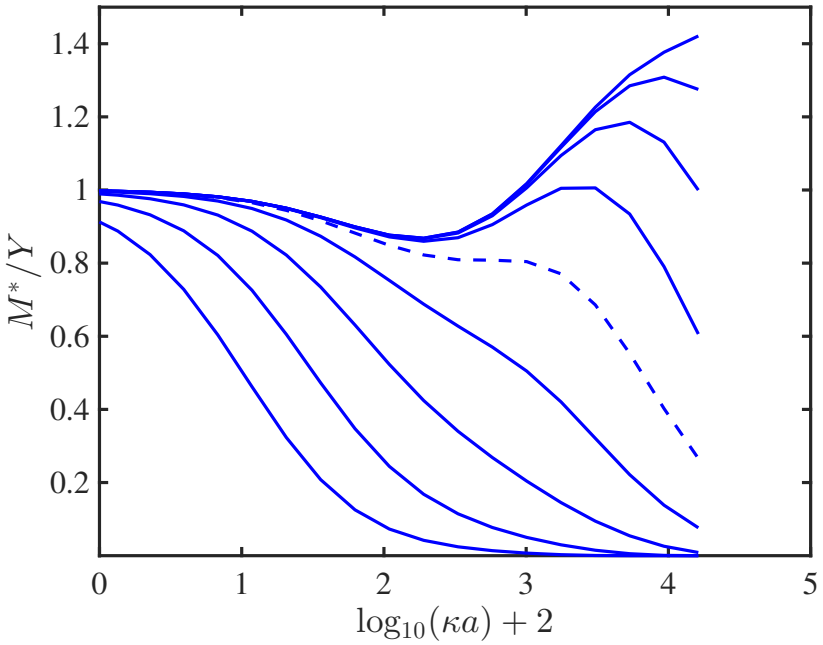

Figure 4.9: Model validation by reproduction of fig. 3 of Allison et al. (2007). Scaled mobility over particle surface potential versus $\log_{10}(\kappa a)+2$ with relaxation effects and $Y = 3$ for charged particles in uncharged gels with Brinkman screening parameter λ/κ = 0, 0.01, 0.027, 0.072, 0.193, 0.519, 1.389, 3.727, 10 (decreasing downward). Dashed line is for $\lambda/\kappa = 0.193$.

.

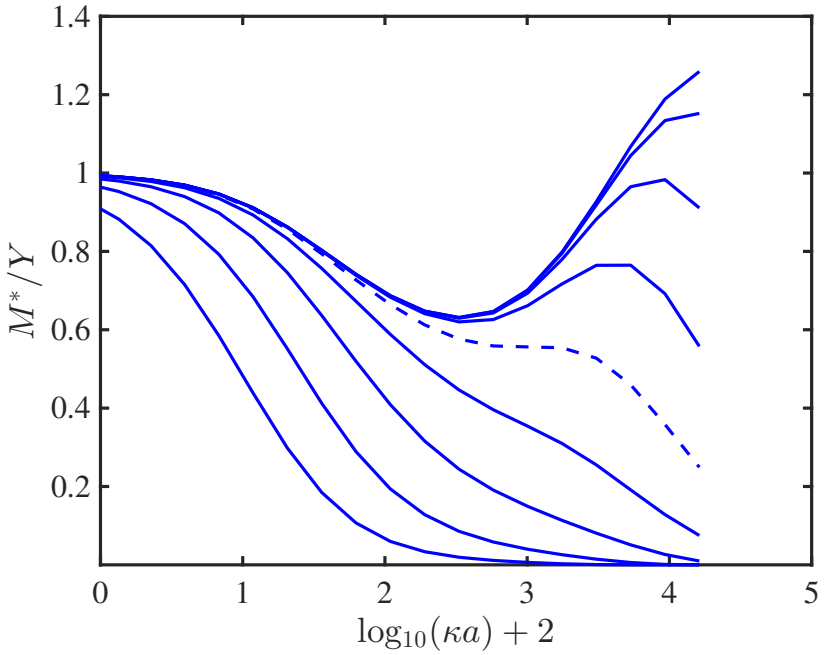

Figure 4.10: Model validation by reproduction of fig. 4 of Allison et al. (2007). Scaled mobility over particle surface potential versus $\log_{10}(\kappa a)+2$ with relaxation effects and $Y = 5$ for charged particles in uncharged gels with Brinkman screening parameter λ/κ = 0, 0.01, 0.027, 0.072, 0.193, 0.519, 1.389, 3.727, 10 (decreasing downward). Dashed line is for $\lambda/\kappa = 0.193$.

.

For weakly charged particles ($Y = 1$), the relaxation effect is not evident. Shown in figs. 4.9 and 4.10, particles with higher surface potentials ($Y = 3, Y = 5$), the relaxation effect is substantial, especially for those with lower gel densities ($\lambda/\kappa = 0$, 0.01, 0.027, 0.072, 0.193). When particles are placed in a denser gel medium (λ/κ = 1.389, 3.727, 10.0), the scaled mobility over surface potential is almost indistinguishable between the three figures. This indicates that a dense gel can attenuate the relaxation effects. Allison et al. (2007) concluded that the gel effect on ion relaxation is only evident for large particles in a dense gel medium, so the relaxation effect is independent of gel concentration for small particles ($\kappa a \leqslant 2$). This conclusion is ob-

vious from fig. 4.11, while the same figure plotted in Allison et al. (2007) might have errors[4].

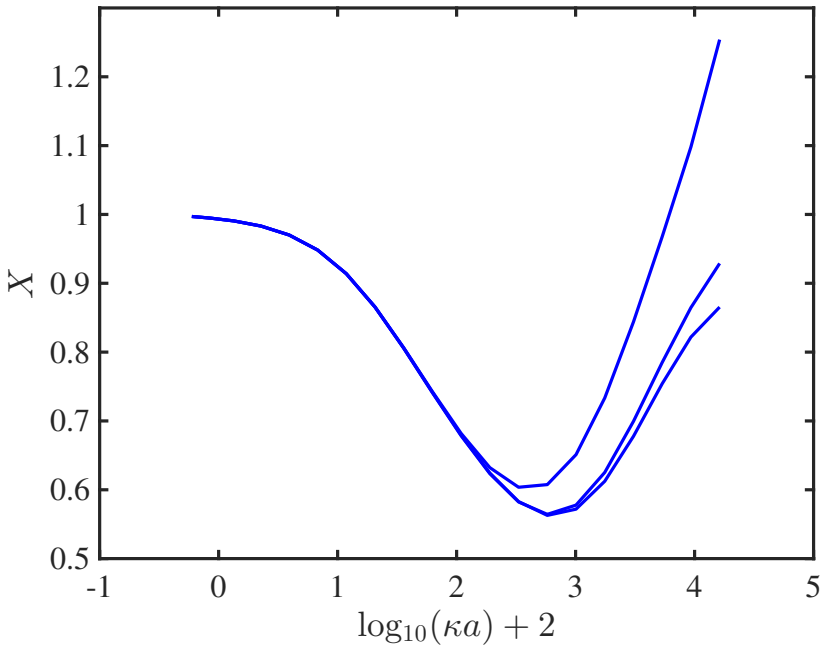

Figure 4.11: X versus $\log_{10}(\kappa a)+2$ for three different values of λ/κ. X is defined as $(M^*/Y)_{Y=5}/(M^*/Y)_{Y=1}$. From the uppermost to lowermost lines, $\lambda/\kappa = 0, 0.193, 1.389$.

.

[4]All data presented in Allison et al. (2007) have evidently been erroneously shifted one unit to the right along the x-axis.

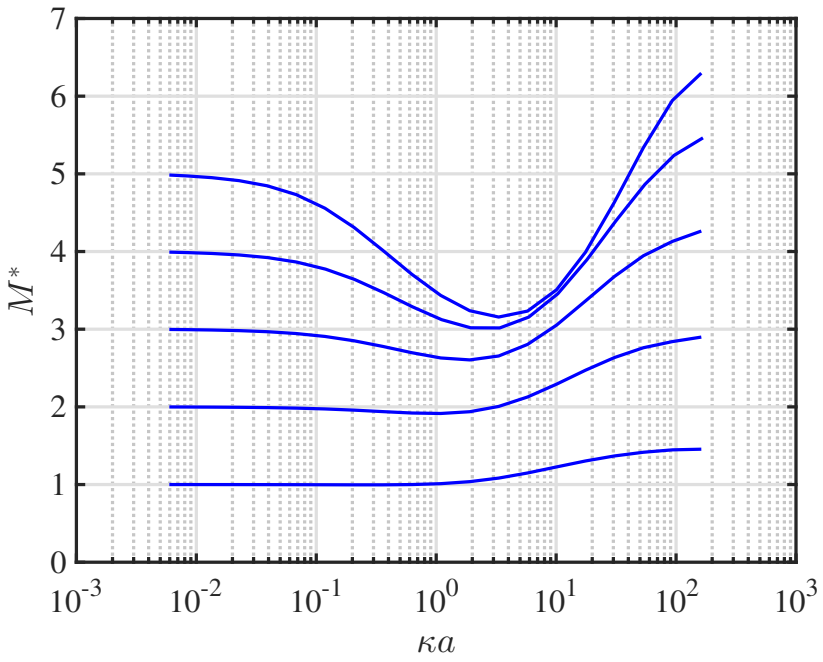

Figure 4.12: Scaled electrophoretic mobility of charged bare particles with surface potentials $Y = 1, 2, 3, 4, 5$ (increasing upward) translating in a free solution versus κa.

.

Allison et al. (2007) further applied their electrokinetic model to interpret experimental gel electrophoresis data for gold nanoparticles from fig. 1 of Zanchet et al. (2002). It is found that Allison's model has good performance in interpreting gel electrophoretic mobility for gold nanoparticles at gel concentrations below 3 wt%. Zanchet et al. (2002) reported gel electrophoresis experimental data for Au particles with gel concentrations between 0.5 wt% and 6 wt%. The buffer, 0.5 × TBE, used in separating Au particles is equivalent to the ionic strength of 16.1 mM based on the calculation of Allison et al. (2007). This ionic strength with a particle radius of 5 nm furnishes $\kappa a = 2.08$. Ferguson plots for Au particles are obtained for the considered range of gel concentrations in Zanchet et al. (2002). The logarithmic mobility data presented in Ferguson plots could be converted to mobility ratios, M^*/M_0^*, where

M^* is scaled gel electrophoretic mobility, and M_0^* is the electrophoretic mobility in free solution. This mobility ratio could be conveniently applied to compare with the model prediction, even if actual charges on the Au particle are not specified in the experiment. The reasoning behind this simplification is: (i) the relaxation effect is independent of gel concentration for small particles ($\kappa a = 2.08$ in the present case), (ii) the relaxation effect is canceled when comparing the mobility ratio, so actual charges on the Au nanoparticles are unimportant. The Brinkman screening length and fixed charged density are the two primary parameters to model hydrogels. For uncharged gels, e.g., agarose gels, the gel is characterized by the following physical parameters: m (gel weight concentration), ρ_g (dry gel density), a_s (radius of gel polymer segment), w_s (ratio of dry gel volume to hydrated gel). In the present model, the gel material of interest is agarose with $\rho_g = 1.64$ g/ml (Laurent, 1967), $a_s = 1.9$ nm (Johnson et al., 1995), $w_s = 0.625$ (Djabourov et al., 1989). Felderhof & Deutch (1975) derived the following equations to relate the physical properties of gel to model parameters:

$$n_s \varsigma_s = \frac{\eta}{\ell_2^2}, \tag{4.8}$$

where the friction coefficient ς_s is written:

$$\varsigma_s = 6\pi\eta a_s \left[1 + \frac{a_s}{\ell_2} + \frac{(a_s/\ell_2)^2}{9}\right], \tag{4.9}$$

and n_s is related to the weight concentration of the gel m by

$$m = \frac{4}{3}\pi\rho_g w_s n_s a_s^3. \tag{4.10}$$

With the foregoing Eqn. 4.8 to Eqn. 4.10, the gel Brinkman screening length ℓ_2 is readily calculated with the given weight concentration of the gel. Once the Brinkman screening length is obtained, the generalized electrokinetic model could be applied to compute the gel electrophoretic mobility of the gold nanoparticles. However, it is also necessary to consider the steric interactions between particles and hydrogel, since the electrokinetic model only captures the hydrodynamic interactions. The electrophoretic mobility after accounting for the steric effects can be written (Allison et al., 2007)

$$\mu^* \approx \frac{1}{1 + 2\phi_{ex}/3} M^*, \tag{4.11}$$

where ϕ_{ex} is the volume excluded to penetration by the spherical particle; it can be written

$$\phi_{ex} = \left(1 + \frac{a}{a_s}\right)^2 \frac{m}{\rho_g w_s}. \tag{4.12}$$

Recall, a is the particle radius, a_s is radius of gel polymer segment, and $f_g = 2\phi_{ex}/3$ is a term that accounts for the steric effects.

We applied the foregoing protocol to calculate the mobility ratio (μ^* relative to the mobility in free solution) of the Au particles over a wide range of gel concentrations. The calculations of the electrophoretic mobility for gold nanoparticles are summarized in tables 4.1 and 4.2. These again confirm that the mobility ratio μ^*/M_0^* is not affected by particle surface potential. The model predictions are compared with gel electrophoresis data from Zanchet et al. (2002), and plotted in fig. 4.13. As

expected, the electrokinetic model has good performance for dilute gels. The nanoparticle electrophoretic mobility decrease substantially with increasing gel concentration. However, the model prediction tends to underestimate the nanoparticle mobility at higher gel concentrations. This is expected, since steric effects accounted for in this model are only valid for dilute gels. Fig. 4.14 is an illustration of the roles of gel steric effects and hydrodynamic effects affecting the particle mobility over a range of gel concentrations. Based on fig. 4.14, the hydrodynamic effects have almost the same magnitude as the gel steric effects in the considered ranges of gel concentration. These results are counterintuitive, because the Brinkman screening lengths shown in tables 4.1 and 4.2 are even smaller compared to the particle radius at high gel concentrations. At this condition, the gel steric effects must dominate over the hydrodynamic effects. Allison et al. (2007) concludes that this is a good interpretation of the gel electrophoresis data, which is questionable. Agarose gels have been treated as an uncharged gel in this model, which is contradictory to earlier literature (Hanauer et al., 2007; Doane et al., 2010), where electro-osmotic flow is observed in agarose gels. Moreover, the Brinkman screening lengths presented in tables 4.1 and 4.2 are also not consistent with experimental results. Johnson & Deen (1996) carefully measured the hydraulic permeability of agarose gels, reporting the gel Brinkman screening length: (1) 1.9 vt% agarose: $\ell_2 = 25$ nm (2) 3.8 vt% agarose: $\ell_2 = 12$ nm (3) 5.5 vt% agarose: $\ell_2 = 7$ nm (4) 7.2 vt% agarose: $\ell_2 = 5$ nm. Holmes & Stellwagen (1990) reported a Brinkman screening length $\ell_2 = 100$ nm for a 1 wt% agarose gels. The calculation based on Eqns. 4.8–4.10 employed in Allison et al. (2007) underestimate the Brinkman screening length for all gel concentrations, which would lead to

stronger hydrodynamic interactions between particles and gel medium. In conclusion, this analysis confirms that the hydrodynamic effects have been overestimated by inaccurate calculations of the gel Brinkman screening length at all gel concentrations, while the electro-osmotic velocity produced by agarose gels also partly contributes to the decreasing electrophoretic mobility with the gel concentrations.

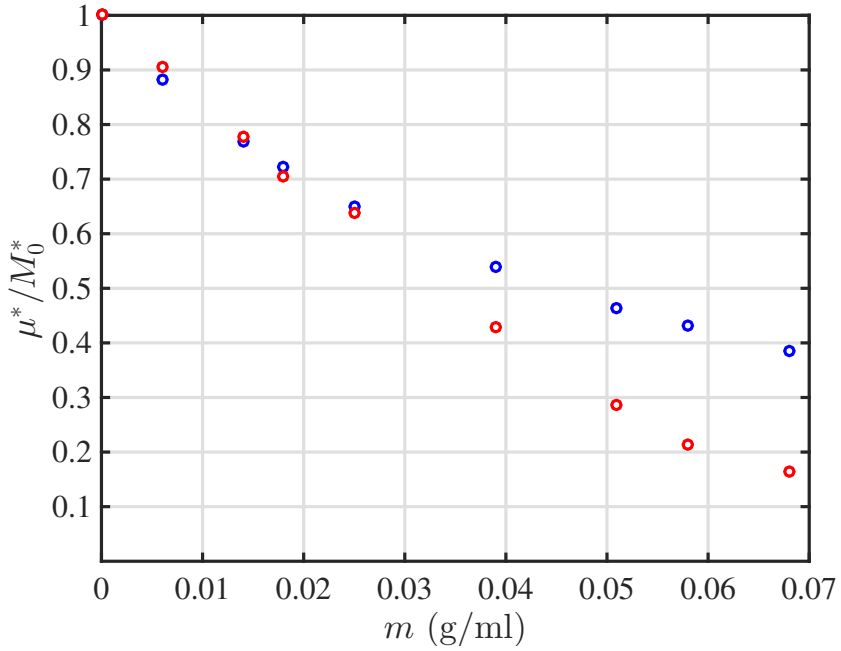

Figure 4.13: Scaled mobility ratio μ^*/M_0^* of gold nanoparticles ($a = 5$ nm) in various weight concentrations of gel. Blue circles are the model predictions, and the red circles the experimental gel electrophoresis data from Zanchet et al. (2002).

.

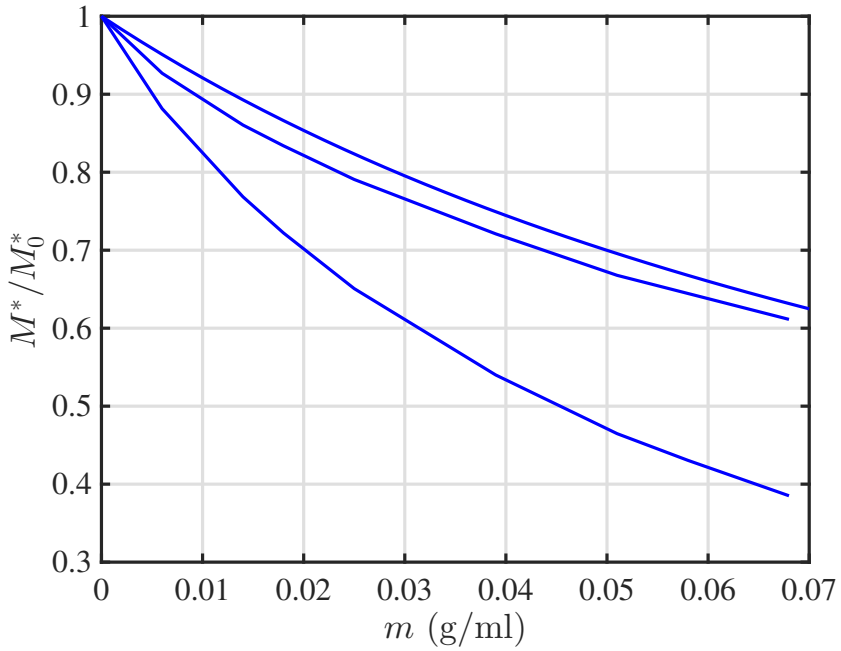

Figure 4.14: Scaled mobility ratio M^*/M_0^* of gold nanoparticles ($a = 5$ nm) in various weight concentrations of gel accounting for: (i) gel steric effects, (ii) gel hydrodynamic effects, and (iii) gel steric and hydrodynamic effects, from uppermost to lowermost.

.

Table 4.1: Calculation of the mobility ratio after accounting for steric effects for gold nanoparticles with dimensionless surface potential $Y = 4$.

$Y = 4$					
m (g/ml)	ℓ_2 (nm)	f_g	M^*	μ^*	μ^*/M_0^*
0.000	-	-	3.01	-	1.00
0.006	10.80	0.951	2.79	2.65	0.88
0.014	6.75	0.893	2.59	2.31	0.77
0.018	5.85	0.866	2.51	2.17	0.72
0.025	4.83	0.823	2.38	1.96	0.65
0.039	3.70	0.749	2.17	1.63	0.54
0.051	3.13	0.696	2.01	1.40	0.46
0.058	2.88	0.668	1.94	1.30	0.43
0.068	2.60	0.630	1.84	1.16	0.39

Table 4.2: Calculation of the mobility ratio after accounting for steric effects for gold nanoparticles with dimensionless surface potential $Y = 1$.

$Y = 1$					
m (g/ml)	ℓ_2 (nm)	f_g	M^*	μ^*	μ^*/M_0^*
0.000	-	-	1.04	-	1.00
0.006	10.80	0.951	0.97	0.93	0.89
0.014	6.75	0.893	0.90	0.87	0.77
0.018	5.85	0.866	0.87	0.84	0.72
0.025	4.83	0.823	0.82	0.79	0.65
0.039	3.70	0.749	0.75	0.72	0.54
0.051	3.13	0.696	0.69	0.66	0.46
0.058	2.88	0.668	0.67	0.64	0.43
0.068	2.60	0.630	0.63	1.16	0.38

4.3 Gel electrophoresis of "soft" nanoparticles with uniform coatings

Having extensively studied the gel effect, our attention is now focused on how to model the corona of soft nanoparticles. The corona structure can be characterized by a non-uniform distribution of segments and charges in the generalized electrokinetic model, while those having uniform coatings would be a specific type of nanoparticle. The theoretical interpretations of gel electrophoresis for this specific soft nanoparticle have been studied by Allison et al. (2016). Here, the model of Hill is used to examine the gel electrophoretic mobility of this specific nanoparticle. The nanoparticles considered have the following physical properties: particle radius $a = 4$ nm, corona thickness $\delta_1 = 2$ nm, with corona having a uniform fixed charge density $\rho_1 = 0$ and Brinkman screening length $\ell_1 = 1$ nm. The particle core is usually set as either uniformly charged or having a uniform surface potential. In the present case, the particle is prescribed with a constant net valance Z (uniformly charged), where $eZ = 4\pi a\sigma_p^2$ with σ_p the surface charge density (MC m^{-3}). The external hydrogel has a uniform Brinkman screening length $\ell_2 = 14.33$ nm, and a uniform charge density $\rho_{f,2}$, from the complete dissociation of H^+.

A complementary error function is used to prescribe the radial distribution of the segment density profile (Hill, 2016):

$$n_s(r) = n_{s,0}0.5\text{erfc}[-(r - L - a)/\delta]. \tag{4.13}$$

When $\delta/L \to 0$, the number density of polymer segments is a perfectly "step-like"

distribution. Fig. 4.15 shows the relation between the number density of polymer segments and the radial distance from the particle surface for uniform coatings with $\ell_1 = 1$ nm when $\delta/L = 0.01$. In the present problem, the dimensionless relative electrophoretic mobility $M^* - M^*_{eo}$ is considered, where M^*_{eo} produced by electroosmotic flow in the charged gel (Allison et al., 2016; Hill, 2016):

$$M^* - M^*_{eo} = \frac{3\eta e}{2\epsilon k_B T} \frac{V - U_{eo}}{E},$$

where U_{eo} is the far-field flow velocity driven by the charged gel.

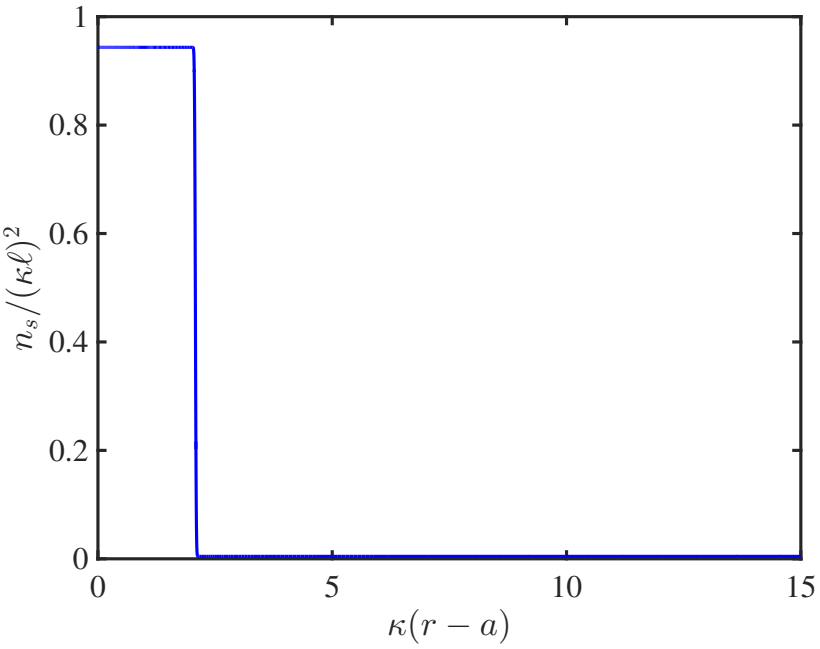

Figure 4.15: The step-like coatings modeled using the complementary error function with $\delta/L = 0.01$.

.

Fig. 4.17 is a reproduction of fig. 4 in Allison et al. (2016) for particles ($Z = -9.8, -19.6, -39.2$) translating in gels ($\rho_{f,2} = 0, -0.005$ MC m^{-3}) with (solid lines) and without (dashed lines) accounting for the relaxation effects. The calculations

demonstrate excellent agreement, also successfully extending the calculations to extremely small κa values ($\kappa a \approx 10^{-2}$), which could not be achieved with Allison's simulation method. The Hückel approximation, rarely addressed in literature for small particles, due to the difficulties encountered in numerical calculations for small κa, are realized in these calculations when $\kappa a \approx 10^{-2}$. Similar to bare particles, the Hückel approximation for soft particles is also achieved by balancing the particle hydrodynamic drag forces $-6\pi\eta a_h(V - U_{eo})$ and Coulomb forces ZeE. Here, Z is the prescribed particle net valence in the present problem. Recall, the hydrodynamic radius $a_h = Fa$, and F is the particle drag coefficient. For soft nanoparticles, the drag coefficient is a complicated function of $F = f(\ell_1, \ell_2, a)$ (Hill & Li, 2013). The calculation of drag coefficient F could be undertaken by the electrokinetic model, and results are plotted over a range of κa values for those soft nanoparticles in fig. 4.16. All those soft nanoparticles without accounting for the relaxation effects have a constant drag coefficient $F = 1.699$ as the red dashed lines shown in fig. 4.16. All those gel electrophoresis calculations that account for the relaxation effects approach to the same drag coefficient when κa becomes smaller. However, for charged gels illustrated in fig. 4.16, the minimum ionic strength can be achieved corresponds to $\log_{10}(\kappa a)+2 \approx 0.75$, where the drag coefficients of highly charged ($Z = -19.6, -39.2$) soft nanoparticles have not converged to $F = 1.699$. The dimensionless relative mobility plotted in fig. 4.17 have already accounted for the gel steric effect $f_g = 0.1139$ reported by (Allison et al., 2016). It is worth to address that the dimensionless relative mobility converges to the same value for particles having same net valance with and without accounting the relaxation effects at vanishing ionic strength.

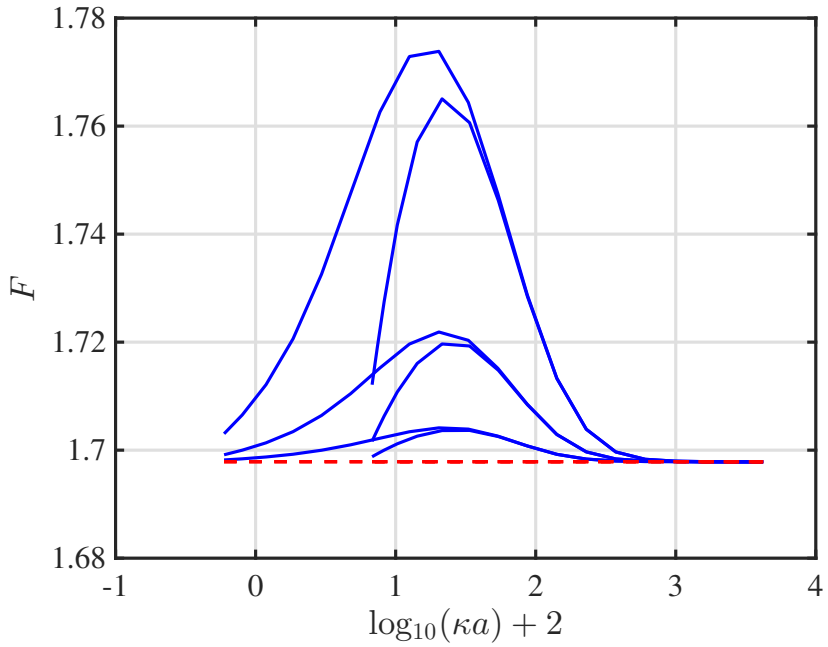

Figure 4.16: F versus $\log_{10}(\kappa a) + 2$ for soft nanoparticles with uniform coatings translating in a gel solution. Red dash line is the Brinkman formula, blue solid lines with a lower limit at about 0.75 on the x-axis correspond to $\rho_{f,2} = -0.005$ MC m^{-3} with $Z = -9.8, -19.6, -39.2$ (from lowermost to uppermost). The other three blue solid lines correspond to $\rho_{f,2} = 0$ with $Z = -9.8, -19.6, -39.2$ (from lowermost to uppermost). Parameters are same as in fig. 4.17.

.

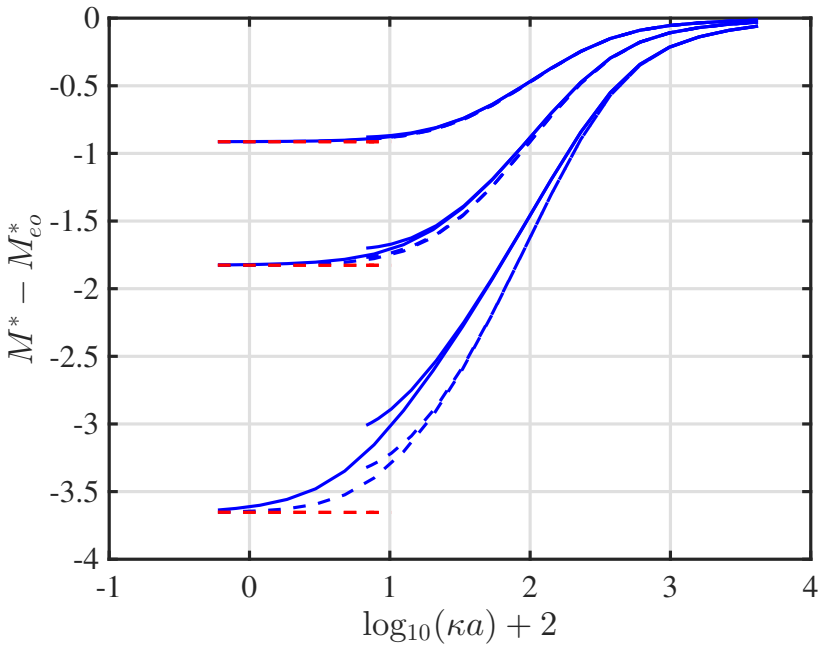

Figure 4.17: $M^* - M^*_{eo}$ versus $\log_{10}(\kappa a) + 2$ for soft nanoparticles with uniform coatings translating in gel medium. Parameters are the same as prescribed in Allison et al. (2016): particle core radius $a = 4.05$ nm, uniform corona thinkness $\delta_1 = 2$ nm, corona Brinkman screening length $\ell_1 = 1$ nm, gel Brinkman screening length $\ell_2 = 14.33$ nm, gel steric effect $f_g = 0.1139$. Blue dashed lines are the relative mobilities without considering the relaxation effects, while blue solid lines included the relaxation effects. Blue solid lines with a lower limit at about 0.75 on the x-axis correspond to $\rho_{f,2} = -0.005$ MC m^{-3} with $Z = -9.8, -19.6, -39.2$ (from uppermost to lowermost). The other three blue solid lines correspond to $\rho_{f,2} = 0$ with $Z = -9.8, -19.6, -39.2$ (from uppermost to lowermost). Red dashed lines are the Hückel approximation.

.

4.4 Gel electrophoresis of PEGylated nanoparticles with peripheral charge

In previous sections, the generalized electrokinetic model was successfully applied to compare with three different independent calculations from the literature. In this section, the theoretical model is used to interpret gel electrophoresis data of PEGylated nanoparticles. Hanauer et al. (2007) conducted a gel electrophoresis experiment to study how the PEGylated nanoparticle mobility varies with the fraction χ of SH-PEG-COOH to SH-PEG-OCH_3 in a 0.5 wt% hydrogel. Hill et al. (2015) have theoretically interpreted these gel electrophoresis data using a free-solution electrokinetic model. They predicted that the gel electrophoretic mobility increase at a lower rate with the increasing fraction χ of charged to uncharged PEG ligands. While this captured the general trend, then remained a notable discrepancy with the experimental data at the lower and higher fraction χ. Hanauer et al. (2007) explained that the mobility reaches to a plateau when $\chi > 0.8$, because the particle steric interactions take effect due to the increasing layer thickness arriving from electrostatic repulsion with large χ. Based on the light-scattering data of the nanoparticles, Hill et al. (2015) argued that the steric interactions are unlikely to have significant influences. Moreover, the rapid increase of mobility at χ near 0 has not been well explained. As for the mobility increasing at a lower rate with respect to the fraction χ, Hill et al. (2015) suggested that it could be explained by the stronger electro-osmotic flow that accompanies the increasing fixed charge on the nanoparticle corona. Apart from these two effects, the gel hydrodynamic effects can not be overlooked. In the present problem, 0.5 wt%

agarose is a dilute hydrogel. When determining the Brinkman screening length ℓ_2, the effective pore size depends on the methods used. Johnson et al. (1995) developed a new technique using the reinforced membrane to measure the gel hydrodynamic permeability. They proposed an empirical formula to for the hydrodynamic permeability of agarose gel:

$$\ell_2^2 = 0.0244\phi^{-2.45},$$

where $\phi = m/\rho_g w_s$ is the hydrogel volume concentration. Recall, $\rho_g = 1.64$ g/ml is the dry gel density, $w_s = 0.625$ is the ratio of the dry gel volume to the hydrated gel volume, and m is the hydrogel weight concentration. Based on this formula, a 0.5 wt% gel has an effective pore size $\ell_2 \simeq$103 nm. Jackson & James (1986) proposed a model that can be used to predict the hydrodynamic permeability of various gels:

$$\frac{\ell_2^2}{a^2} = -\frac{3}{20\phi}(\ln\phi + 0.931),$$

where ϕ is the hydrogel volume concentration, and a_s is the gel polymer segment radius. According to this formula, the Brinkman screening length of a 0.5 wt% gel is $\ell_2 \simeq 22$ nm, while this prediction is significantly smaller than the previous one. Johnson et al. (1995) explained that the discrepancy at the small concentrations could be attributed by an increase of polymer segment radius.

Ferguson plots are also widely adopted to estimate the effective pore size of gels. These are semi-logarithemic plot of electrophoretic mobility versus gel concentrations for DNA molecule (Slater et al., 1988). Applying Ferguson plot method, Holmes & Stellwagen (1990) found that the median pore size of a 0.6 wt% agarose gel is $\ell_2 \simeq 160$ nm. Serwer & Hayes (1986) applied the gel electrophoresis to determine the effective

pore size of agarose gels based on the exclusion effects of spheres in agarose gels. They reported that the effective pore size of agarose gels is well captured by:

$$\ell_2 = 118C^{-0.74} \qquad \text{with} \qquad 0.2<C<4,$$

where C(%) is the gel weight concentrations. This furnishes for a 0.5 wt% agarose gel an effective pore size of 197 nm.

Atomic force microscopy (AFM) is also an important tool for probing gel structure. Maaloum et al. (1998) estimated the pore diameters of various concentrations of agarose gel from AFM images. They concluded that gel pore diameter has a wider distribution at lower concentrations: a 0.5 wt% gel solution has a median pore size of 810 nm. Stellwagen (2009) reviewed that the gel pore size measured by AFM methods tend to be larger than the value determined by electrophoresis. They speculated that the effective pore size of a gel determined by gel electrophoresis is more relevant for interpreting gel electrophoresis. Based on the above review, a conservative estimate of the Brinkman screening length for 0.5 wt% agarose gels would be between 100 and 200 nm.

Nanoparticle corona structure is complicated, Hill et al. (2015) assume polymer segments and fixed charge densities having a radial distribution with Gaussian functions. Several unknown parameters (see Eqns. 4.1-4.4) need to be determined in Gaussian functions to model the corona structure. Appropriately setting these parameters enables a gel electrophoresis model to predict the nanoparticle electrophoresis data. They conducted free-solution electrophoresis experiments for CM-5kPEG-Au NPs (a = 2.7 nm) at various ionic concentrations. The electrophoretic mobilities

for CM-5kPEG-Au NPs were used to fit the parameters in the Gaussian functions. Two parameters were specifically addressed: the nanoparticle layer thickness δ_1 (see fig. 4.2), and the position of corona maximum charge density L_2 (see fig. 4.2). The nanoparticle is negatively charged with a core surface charge density $\sigma_p = -15$ mC m^{-2}. The dissociation of H^+ from PEG ligands would also made it negatively charged. These equally signed charges have a strong repulsion effect that repells the terminally anchored charge from the core. Thus, the corona geometry parameter L_2 is expected to be larger than δ_1. For layer thickness δ_1, the electrostatic interaction between polymer chain ends and nanoparticle core would increase the layer thickness. The layer thickness is influenced by the ionic strength, since the screening effect that directly relates to ionic strength would reduce the electrostatic interaction between chain ends and the nanoparticle core. To account for the influence of ionic strength on the PEG layer thickness, Hill et al. (2015) prescribed an interpolating formula:

$$L/L_0 = (L_\infty/L_0 - 1)/(I/I_0 + 1) + 1, \tag{4.14}$$

where L is the layer thickness δ_1, L_∞ is the maximum layer thickness achieved at vanishing ionic strength, L_0 is the minimum layer thickness achieved at high ionic strength, and I_0 is the transition ionic strength. Apart from the geometry parameters in Gaussian functions, appropriately setting the hydrodynamic segment size a_s is also essential to quantitively interpret the electrophoresis data of CM-5kPEG-Au NPs. The hydrodynamic drag size a_s and segment density n_s together determine the corona permeability ℓ_1^2, where a larger corona permeability would furnish a smaller hydrodynamic particle radius and a higher mobility. The Brinkman screening length

$\ell_1(r)$ of polymer segment is furnished by equating the drag force on a single segment $\boldsymbol{f}_s = 6\pi\eta a_s(\boldsymbol{u} - \boldsymbol{V})F_s(\phi)$ and the so-called Darcy-drag $(\eta/\ell_1^2)(\boldsymbol{u} - \boldsymbol{V})$ (Hill et al., 2003a), giving

$$\ell_1^2(r) = \frac{1}{6n_s(r)\pi a_s F_s(\phi)},$$

where $F_s(\phi)$ is the segment drag coefficient, and $\phi = n_s 4\pi a_s^3/3$ is the segment volume fraction. The relation between $F_s(\phi)$ and ϕ is shown in fig. 5.1 in the Appendix. The choice of the number of segments in a chain is arbitrary in the electrokinetic model when interpreting the free-solution electrophoretic mobility for soft nanoparticles. For convenience, Hill et al. (2015) treated a polymer chain as one segment ($N_s = 1$), with segment hydrodynamic radius $a_s = 1.7$ nm, cora radius $a = 2.7$ nm, core surface charge density $\sigma_p = -15$ mC m^{-2}, number of ligands $N_a = 146$, and corona geometry parameters set as follows: corona thickness $\delta_1 = L$ (from Eqn. 4.14, with $L_\infty = 18$ nm, $L_0 = 4$ nm, $I_0 = 1$ mM), the radial position of the maximum segment density $L_1 = 0$, the radial position of the maximum charge density $L_2 = 3\delta_1/2$, and corona charge density distribution $\delta_2 = \delta_1/3$, they successfully interpreted the electrophoretic mobility for CM-5kPEG-Au NPs in free solution. However, the arbitrary choice of the number of segments in a chain is questionable when the gel effect is accounted for. This is discussed as follows. Here, the radial profile of segment concentration n_s is replotted (see fig. 5.2 in the Appendix) when layer thickness $\delta_1 = 4.14$ nm, which is the thickness at ionic strength $I = 100$ mM according to Eqn. 4.14. This figure is consistent with the fig. 2 in Hill et al. (2015). Moreover, the radial profile of the segment volume fraction ϕ can be readily obtained with the given radial profile of n_s.

Interestingly, the radial profile of the segment volume fraction ϕ shown in fig. 5.3 has a volume fraction larger than one near the particle surface. This indicates that the number of segments in a chain ($N_s = 1$) is not realistic, though these parameters could enable the model to give a satisfactory prediction to the experimental electrophoretic mobility data. Therefore, we performed the calculation with a larger number of N_s ($N_s = 4$), accordingly with a slight adjustment of the segment radius ($a_s = 0.7$ nm) and corona geometry parameters ($L_\infty = 15$ nm). The electrokinetic model can still reproduce the "knee" as shown in fig. 4.18. The figure is consistent with the calculation of the electrophoretic mobilities for CM-5kPEG-Au NPs with $N_s = 1$. The adjustment of the model parameters significantly increases the number density of segments at each radial position (see fig. 5.5 in the Appendix), also decreasing the segment volume fraction to reasonable values (see fig. 5.6 in the Appendix).

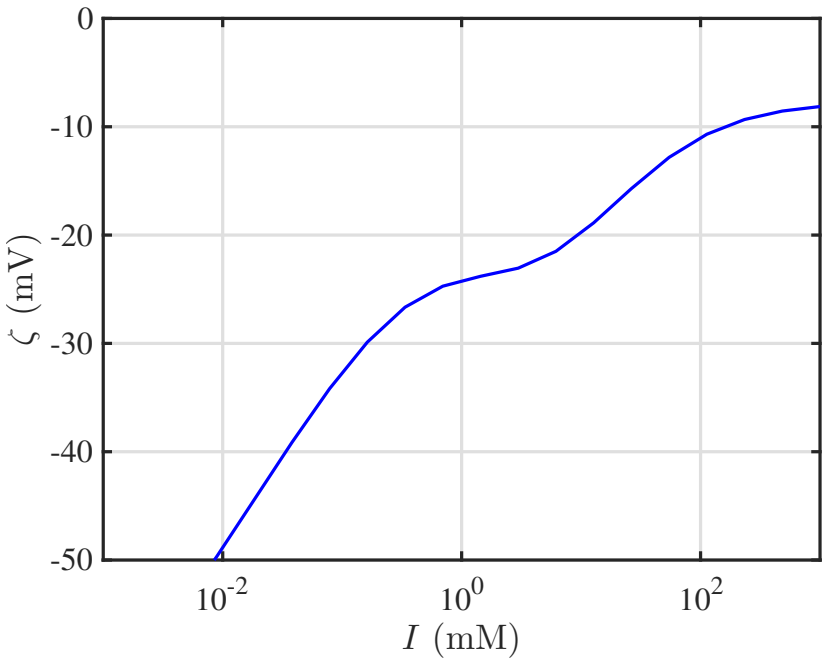

Figure 4.18: Calculation of free-solution electrophoretic mobility for CM-5kPEG-Au NPs ($a = 2.7$ nm) with $N_s = 4$, $a_s = 0.7$ nm. Electrophoretic mobility reported as a Smoluchowski ζ potential (mV) versus ionic strength I (mM). The line passes through the experimental data shown in Hill et al. (2015).

.

Based on these parameter settings for the PEG ligand, the electrophoretic mobility of the PEGylated NPs of Hanauer et al. (2007) is examined to help understand the model interpretation of the electrophoretic mobility at small and large fractions χ. As presented in fig. 3 of Hill et al. (2015), PEGylated NPs ($a = 10$ nm, $N_a = 2010$) have a hydrodynamic radius $a_h \approx 21$ nm, that is significantly smaller than the Brinkman screening length ℓ_2 of 0.5 wt% agarose gels. The gel steric effects anticipated by Hanauer et al. (2007) are unlikely to be significant with such a large gel pore size 100 $\sim$ 200 nm, whereas the gel hydrodynamic effects on the nanoparticle mobility can not be overlooked. Moreover, the electrostatic repulsion between chain ends and the particle core could increase the average layer thickness with the increasing fraction χ

of univalent charged PEGylated ligand. This might be significant in influencing the nanoparticle mobility. The generalized electrokinetic model was applied to account for the gel hydrodynamic effects to interpret the electrophoretic mobility of PEGylated NPs ($a = 10$ nm, $N_a = 2010$) with varying fractions of charged PEGylated ligands. As shown in fig. 4.19, this model predicts the average layer thickness increasing linearly from 3.0 nm to 6.22 nm with χ when Brinkman screening length $\ell_2 = 110$ nm. Note that a mobility 0.315 μm cm s^{-1} V^{-1} is added to the experimental mobility data of Hanauer et al. (2007) to account for electro-osmotic flow in the gel.

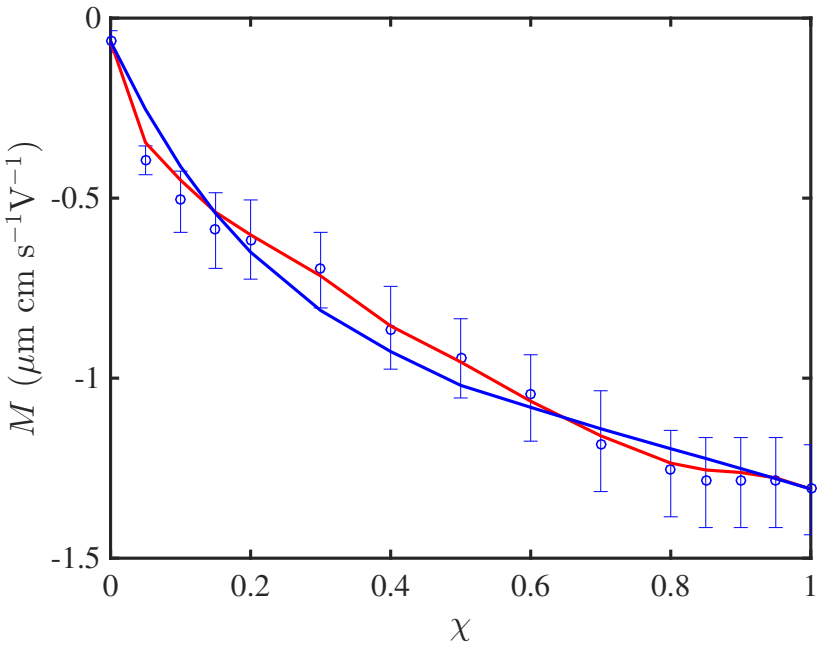

Figure 4.19: Electrophoretic mobility (μm cm s^{-1} V^{-1}) of PEGylated nanoparticles with $N_s = 4$, $a_s = 0.7$ nm versus the fraction χ of charged PEG chains in a 0.5 wt% agarose gel. Error bars are the gel electrophoresis experimental data from Hanauer et al. (2007). A mobility 0.315 μm cm s^{-1} V^{-1} is added to all data to account for electroosmotic flow in the gel (Hanauer et al., 2007). Blue line is the theoretical prediction for a nanoparticle layer thickness that increases linearly from 3.0 nm to 6.22 nm with χ. Red line corresponds to the circles in fig. 4.20.

.

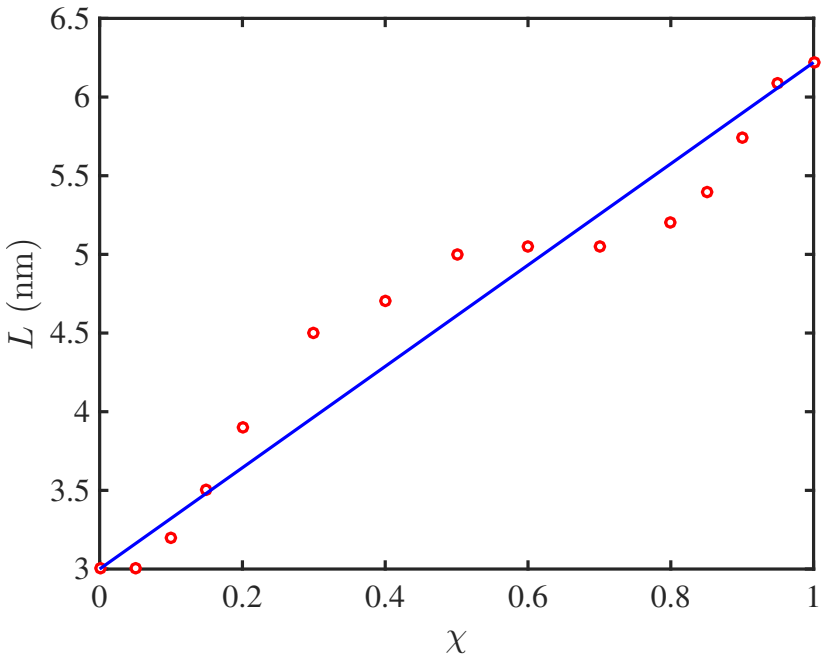

Figure 4.20: Averaged nanoparticle layer thickness versus the fraction χ of charged PEG chains. Blue line is the assumption that the averaged nanoparticle layer thickness increases linearly with the fraction χ of charged PEG chains. Red circles are for nanoparticle layer thickness at a given χ that furnishes the best fit to experimental data in fig. 4.19.

.

According to the scaling/blob theory of Biver et al. (1997), the layer thickness for uncharged polymers are determined by the grafting density and substrate curvature. A weaker curvature of univalent PEGylated nanoparticles at the same grafting density would furnish a larger layer thickness, although the layer is polyelectrolyte rather than uncharged polymer. Based on this principle, the layer thickness $\delta_1 = 6.22$ nm of the charged PEG NPs ($a = 10.0$ nm) is reasonable, since CM-5kPEG-Au NPs ($a = 2.7$ nm) with the same grafting density have a smaller layer thickness $\delta_1 = 4.52$ nm at ionic strength $I = 20$ mM. From figs. 4.19 and 4.20, we may conclude that changes in the layer thickness have a significant impact on the nanoparticle mobility. To address

the hydrodynamic effect of gel, the electrophoretic mobility of the PEGylated NPs at fraction χ=1 with gel Brinkman screening length l_2 = 1000 nm (mimicking free-solution electrophoresis) are calculated. A higher mobility ($M = 1.7$ μm cm s^{-1} V^{-1}) is obtained without accounting for the gel hydrodynamic effect, suggesting that 0.5 wt% agarose gel has a significant effect in retarding nanoparticle mobility.

However, treating each polymer chain as a collection of N Kuhn segments, each with Kuhn length l, is more realistic. The length of a fully stretched chain is $L = Nl$ for the Kuhn segment chain. The number of Kuhn segments for 5 kDa PEG chain is $N = 83$ (Hill et al., 2015). Again, the calculations are performed for the free-solution electrophoretic mobility of CM-5kPEG-Au NPs (a = 2.7 nm) to fit the parameters in the Gaussian functions when a polymer chain has Kuhn segments. With a larger number of segments N_s in a chain, the hydrodynamic radius of each segment must be smaller to have a comparable drag force exerted on the fluids. By fitting the model to the electrophoresis data for CM-5kPEG-Au NPs (a = 2.7 nm) in fig. 1 of Hill et al. (2015), the following adjustments are necessary: segment hydrodynamic radius changes to a_s = 0.07 nm, corona geometry parameters change to L_∞ = 15 nm, and L_0 = 3.5 nm (see fig. 5.8 in the Appendix). As expected, when the number of segments in a chain increases from $N_s = 4$ to $N_s = 83$, the segment density n_s increases significantly (see fig. 5.9 in the Appendix), while the segment volume fraction decreases to a value close to 0 (see fig. 5.10 in the Appendix). The segment drag coefficient $F_s(\phi)$ is close to one at such small segment volume fractions ϕ. The drag exerted on each segment is therefore approximately equal to the well known Stokes drag force, which is consistent with early studies (Hill et al., 2003a). Here, we are

interested in whether the number of Kuhn segments would have significant influence on interpreting the electrophoretic mobilities of the PEGylated NPs of Hanauer et al. (2007). The gel electrophoresis model was applied to calculate the electrophoretic mobilities of PEGylated NPs with varying fractions of charged PEG ligands, also permitting the layer thickness to increase with χ. The gel Brinkman screening length in the calculations remain unchanged ($\ell_2 = 110$ nm). Not surprisingly, allowing the layer thickness increases from 3.0 nm to 6.15 nm with the increasing fraction of charged PEG ligands would furnish a satisfying fit to the experimental mobility data for the PEGylated NPs of Hanauer et al. (2007), as shown in figs. 4.21 and 4.22. However, the particle layer thickness increases more rapidly at small χ. To examine the gel effect on the nanoparticle mobility, the electrophoretic mobility for the nanoparticle bearing fully charged PEG ligand (fraction $\chi = 1$) with gel Brinkman screening length $\ell_2 =$ 1000 nm (mimicking free-solution electrophoresis) was calculated. The nanoparticle mobility obtained at this condition is 1.32 μm cm s^{-1} V^{-1}, which is close to the gel electrophoretic mobility when $\ell_2 = 110$ nm, suggesting that the gel does not have significant effect on the nanoparticle mobility. The conclusion at this condition (N_s = 83) is contradictory to the previous interpretation ($N_s = 4$). This contradiction may be explained by the relation between the segment drag coefficient and segment volume fraction. When a polymer chain has number of segments $N_s = 83$, the small segment volume fraction furnishes a segment drag coefficient close to one. In the presence of a gel, the small changes in the segment volume fraction in the region of polyelectrolyte would not have a substantial influence on the segment drag coefficient. However, according to fig. 5.1, a small addition of polymer segments (due to the gel)

would significantly increase the segment drag coefficient when the segment volume fraction is larger than 0.5. While this is the case for polymer chain with number of segments $N_s = 4$ (see fig. 5.6 in the Appendix).

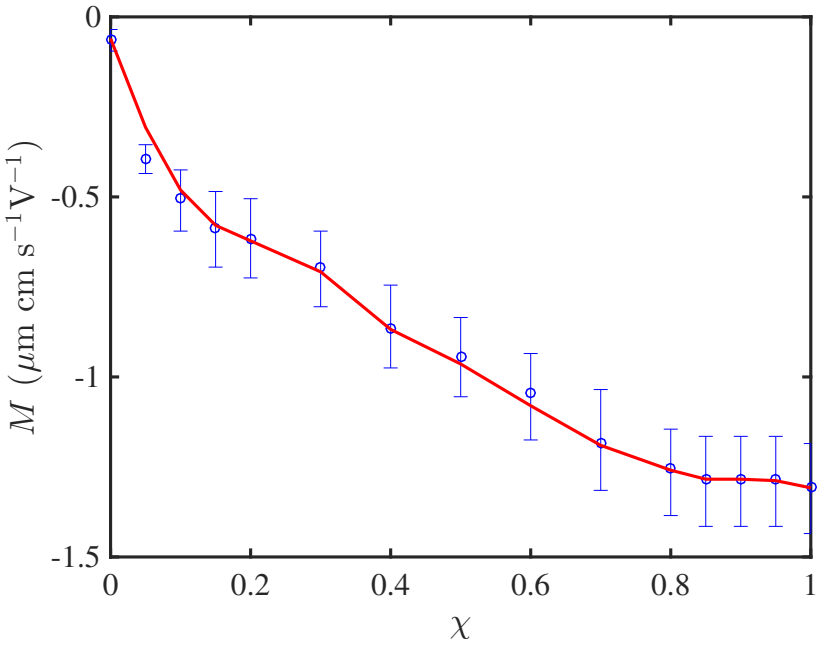

Figure 4.21: Electrophoretic mobility (μm cm s^{-1} V^{-1}) of PEGylated nanoparticles with $N_s = 83$, $a_s = 0.07$ nm versus the fraction χ of charged PEG chains in a 0.5 wt% agarose gel. Error bars are the gel electrophoresis experimental data from Hanauer et al. (2007). A mobility 0.315 μm cm s^{-1} V^{-1} is added to all data to account for electroosmotic flow in the gel (Hanauer et al., 2007). Red line corresponds to the layer thickness in fig. 4.22.

.

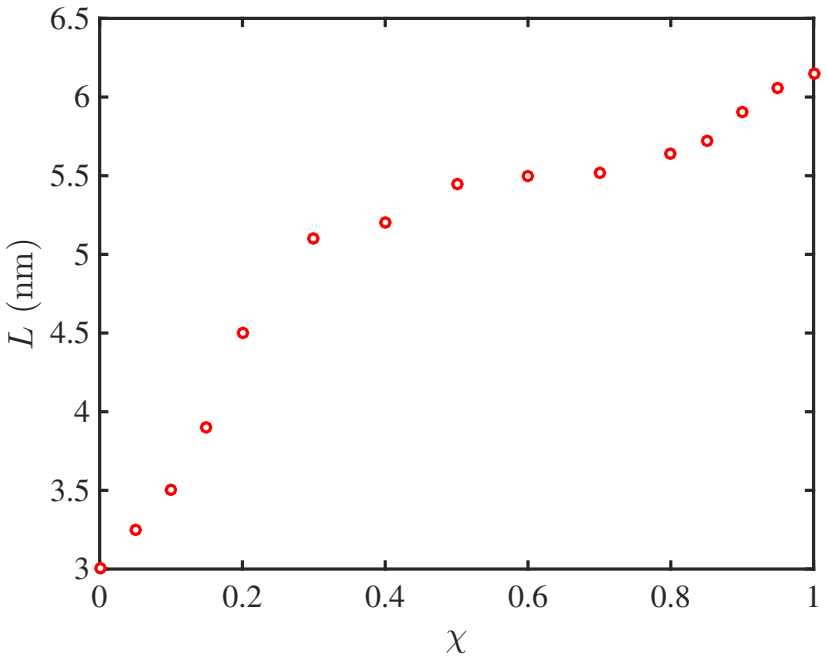

Figure 4.22: Averaged nanoparticle layer thickness versus the fraction χ of charged PEG chains that gives the best fit to experimental data in fig. 4.21. The layer thickness increases from 3.0 nm to 6.15 nm.

.

In conclusion, the theoretical interpretation of the PEGylated NPs of Hanauer et al. (2007) performed by (Hill et al., 2015) could be improved by allowing the layer thickness to increase with the fraction of univalent charged PEG ligand. It is recommended to use Kuhn segments to simulate the polyelectrolyte for interpreting the gel electrophoresis of soft/functionalized nanoparticles. It would also be benefit from experimental studies that test how the nanoparticle polyelectrolyte layer thickness changes with the amount of charge.

Chapter 5

Conclusions

The generalized electrokinetic model recently developed by Hill (2016) has been applied to simulate the gel electrophoresis of spherical nanoparticles translating in gel solutions. The model includes a pH-charge regulation model for polyelectrolytes and hydrogels, and captures the ion concentration perturbation (termed relaxation effects). The applicability of this model has been successfully tested by several direct comparisons to literature calculations, including charge regulated bi-functional particles in uncharged gels (Hsu et al., 2013), highly charged particles in uncharged gels (Allison et al., 2007), and soft nanoparticles with uniform polymer coatings in uncharged and charged gels (Allison et al., 2016). For gel electrophoresis of charge regulated bi-functional particles, a very thin charge-regulated polyelectrolyte is applied to mimic charge regulated particle surfaces. For gel electrophoresis of highly charged particles, the relaxation effects and gel hydrodynamic effects were successfully captured. Soft nanoparticles with uniform polymer coatings are a specific case of this generalized electrokinetic model. The rarely addressed Hückel approximation,

which has not been advanced by Allison et al. (2016) was achieved at $\kappa a \approx 10^{-2}$.

The generalized electrokinetic model was further applied to interpret the gel electrophoretic mobilities of PEGylated NPs reported by Hanauer et al. (2007). A rapid increase in nanoparticle mobility at a small fraction of charged PEG ligands ($\chi \approx 0$) and a plateau at a large fraction of charged PEG ligands ($\chi > 0.8$) could be explained by allowing the layer thickness to increase with the fraction of univalent charged PEG ligands. It is recommended to use Kuhn segments to simulate polyelectrolytes for interpreting the gel electrophoresis of soft nanoparticles. The theoretical model also indicates that gel hydrodynamic effects are not significant for soft nanoparticles in dilute gel solutions. Finally, this theoretical interpretation would benefit from experimental studies that test how the nanoparticle polyelectrolyte layer thickness changes with the amount of charge.

Bibliography

S. Allison, et al. (2016). 'Electrophoretic mobility of a dilute, highly charged "Soft" spherical particle in a charged hydrogel'. *J. Phys. Chem. B* **120**(33):8071–8079.

S. A. Allison, et al. (2014). 'The electrophoretic mobility of a weakly charged "Soft" sphere in a charged hydrogel: Application of the Lorentz Reciprocal theorem'. *J. Phys. Chem. B* **118**(29):8827–8838.

S. A. Allison, et al. (2007). 'Electrophoresis of spheres with uniform zeta potential in a gel modeled as an effective medium'. *J. Colloid Interface Sci.* **313**:328–337.

C. Biver, et al. (1997). 'Neutral and charged polymer brushes: A model unifying curvature effects from micelles to flat surfaces'. *Macromolecules* **30**(6):1787–1792.

H. C. Brinkman (1949). 'A calculation of the viscous force exerted by a flowing fluid on a dense swarm of particles'. *Flow Turbul. Combust.* **1**(1):27.

C. Calladine, et al. (1991). 'A study of electrophoretic mobility of DNA in agarose and polyacrylamide gels'. *J. Mol. Biol.* **221**(3):981–1005.

Y.-Y. Chen, et al. (2014). 'Electrophoresis of pH-regulated, zwitterionic particles:

Effect of self-induced nonuniform surface charge'. *J. Colloid Interface Sci.* **421**:154–159.

P. Couvreur (1988). 'Polyalkylcyanoacrylates as colloidal drug carriers'. *Crit. Rev. Ther. Drug Carrier Syst.* **5**(1):1–20.

P. Debye & A. M. Bueche (1948). 'Intrinsic viscosity, diffusion, and sedimentation rate of polymers in solution'. *J. Chem. Phys.* **16**(6):573–579.

M. Djabourov, et al. (1989). 'Small-angle x-ray scattering characterization of agarose sols and gels'. *Macromolecules* **22**(1):180–188.

T. L. Doane, et al. (2010). 'Electrophoretic mobilities of PEGylated gold NPs'. *J. Am. Chem. Soc.* **132**(44):15624–15631.

B. Felderhof & J. Deutch (1975). 'Frictional properties of dilute polymer solutions. I. Rotational friction coefficient'. *J. Chem. Phys.* **62**(6):2391–2397.

R. Greenwood & K. Kendall (1999). 'Selection of suitable dispersants for aqueous suspensions of zirconia and titania powders using acoustophoresis'. *J. Eur. Ceram. Soc.* **19**(4):479–488.

M. Hanauer, et al. (2007). 'Separation of nanoparticles by gel electrophoresis according to size and shape'. *Nano Lett.* **7**(9):2881–2885.

T. W. Healy & L. R. White (1978). 'Ionizable surface group models of aqueous interfaces'. *Adv. Colloid Interface Sci.* **9**(4):303–345.

D. Henry (1931). 'The cataphoresis of suspended particles. Part I. The equation of cataphoresis'. *Proc. R. Soc. A* **133**(821):106–129.

R. Hill, et al. (2015). 'Electrophoretic interpretation of PEGylated NP structure with and without peripheral charge'. *Langmuir* **31**(37):10246–10253.

R. Hill & D. Saville (2005). ''Exact' solutions of the full electrokinetic model for soft spherical colloids: Electrophoretic mobility'. *Colloids Surf., A* **267**(1-3):31–49.

R. J. Hill (2015a). 'Corona charge regulation in nanoparticle electrophoresis'. *Proc. R. Soc. A* **471**(2183).

R. J. Hill (2015b). 'Hydrogel charge regulation and electrolyte ion-concentration perturbations in nanoparticle gel electrophoresis'. *Proc. R. Soc. A* **471**(2184).

R. J. Hill (2016). 'Electrokinetics of nanoparticle gel-electrophoresis'. *Soft Matter* **12**:8030–8048.

R. J. Hill & F. Li (2013). 'Hydrodynamic drag coefficient for soft core–shell nanoparticles in hydrogels'. *Chem. Eng. Sci.* **89**:1–9.

R. J. Hill, et al. (2003a). 'Electrophoresis of spherical polymer-coated colloidal particles'. *J. Colloid Interface Sci.* **258**:56–74.

R. J. Hill, et al. (2003b). 'Polarizability and complex conductivity of dilute suspensions of spherical colloidal particles with uncharged (neutral) polymer coatings'. *J. Colloid Interface Sci.* **268**(1):230–245.

D. L. Holmes & N. C. Stellwagen (1990). 'The electric field dependence of DNA mobilities in agarose gels: A reinvestigation'. *Electrophoresis* **11**(1):5–15.

J.-P. Hsu, et al. (2013). 'Gel electrophoresis of a charge-regulated, bi-functional particle'. *Electrophoresis* **34**(5):785–791.

E. Hückel (1924). 'Die kataphorese der kugel'. *Physik. Z.* **25**:204–210.

G. W. Jackson & D. F. James (1986). 'The permeability of fibrous porous media'. *Can. J. Chem. Eng.* **64**(3):364–374.

E. M. Johnson, et al. (1995). 'Diffusion and partitioning of proteins in charged agarose gels'. *Biophys. J .* **68**:1561–1568.

E. M. Johnson & W. M. Deen (1996). 'Hydraulic permeability of agarose gels'. *AlChE J.* **42**(5):1220–1224.

T. C. Laurent (1967). 'Determination of the structure of agarose gels by gel chromatography'. *Biochim. Biophys. Acta* **136**(2):199–205.

F. Li, et al. (2014). 'Nanoparticle gel electrophoresis: Soft spheres in polyelectrolyte hydrogels under the Debye–Hückel approximation'. *J. Colloid Interface Sci.* **423**:129–142.

M. Maaloum, et al. (1998). 'Agarose gel structure using atomic force microscopy: Gel concentration and ionic strength effects'. *Electrophoresis* **19**(10):1606–1610.

R. W. O'Brien & L. R. White (1978). 'Electrophoretic mobility of a spherical colloidal particle'. *J. Chem. Soc., Faraday Trans. 2* **74**:1607–1626.

H. Ohshima & T. Kondo (1989). 'Approximate analytic expression for the electrophoretic mobility of colloidal particles with surface-charge layers'. *J. Colloid Interface Sci.* **130**(1):281–282.

J. T. G. Overbeek (1943). 'Theory of electrophoresis-the relaxation effect'. *Kolloid-Beih* **54**:287–364.

A. Pluen, et al. (1999). 'Diffusion of macromolecules in agarose gels: comparison of linear and globular configurations'. *Biophys. J .* **77**:542–552.

P. Serwer & S. J. Hayes (1986). 'Exclusion of spheres by agarose gels during agarose gel electrophoresis: Dependence on the sphere's radius and the gel's concentration'. *Anal. Biochem.* **158**(1):72–78.

G. W. Slater, et al. (1988). 'Quantitative analysis of the three regimes of DNA electrophoresis in agarose gels'. *Biopolymers* **27**(3):509–524.

P. Smejtek, et al. (2010). 'Electrophoretic mobility of sarcoplasmic reticulum vesicles is determined by amino acids of A + P + N domains of Ca^{2+}–ATPase'. *Biochim. Biophys. Acta* **1798**(9):1689–1697.

M. Smoluchwski (1921). 'Electrische endosmose und stromungesstrome (electroosmosis and current flow)'. *In Handbuch der Electrizitat und des Magnetismus* **2**.

I. Sosa, et al. (2003). 'Optical properties of metal nanoparticles with arbitrary shapes'. *J. Phys. Chem. B* **107**(26):6269–6275.

R. Sperling, et al. (2006). 'Electrophoretic separation of nanoparticles with a discrete number of functional groups'. *Adv. Funct. Mater.* **16**(7):943–948.

N. C. Stellwagen (2009). 'Electrophoresis of DNA in agarose gels, polyacrylamide gels and in free solution'. *Electrophoresis* **30**:S188–S195.

D. Stigter (2000). 'Influence of agarose gel on electrophoretic stretch, on trapping, and on relaxation of DNA'. *Macromolecules* **33**(23):8878–8889.

A. Weidner, et al. (2015). 'Preparation of core-shell hybrid materials by producing a protein corona around magnetic nanoparticles'. *Nanoscale Res. Lett.* **10**(1).

P. Wiersema, et al. (1966). 'Calculation of the electrophoretic mobility of a spherical colloid particle'. *J. Colloid Interface Sci.* **22**(1):78–99.

K. Y. Win & S.-S. Feng (2005). 'Effects of particle size and surface coating on cellular uptake of polymeric nanoparticles for oral delivery of anticancer drugs'. *Biomaterials* **26**(15):2713–2722.

D. Zanchet, et al. (2002). 'Electrophoretic and structural studies of DNA-directed Au nanoparticle groupings'. *J. Phys. Chem. B* **106**(45):11758–11763.

B. H. Zimm & S. D. Levene (1992). 'Problems and prospects in the theory of gel electrophoresis of DNA'. *Q. Rev. Biophys.* **25**(2):171–204.

Appendix

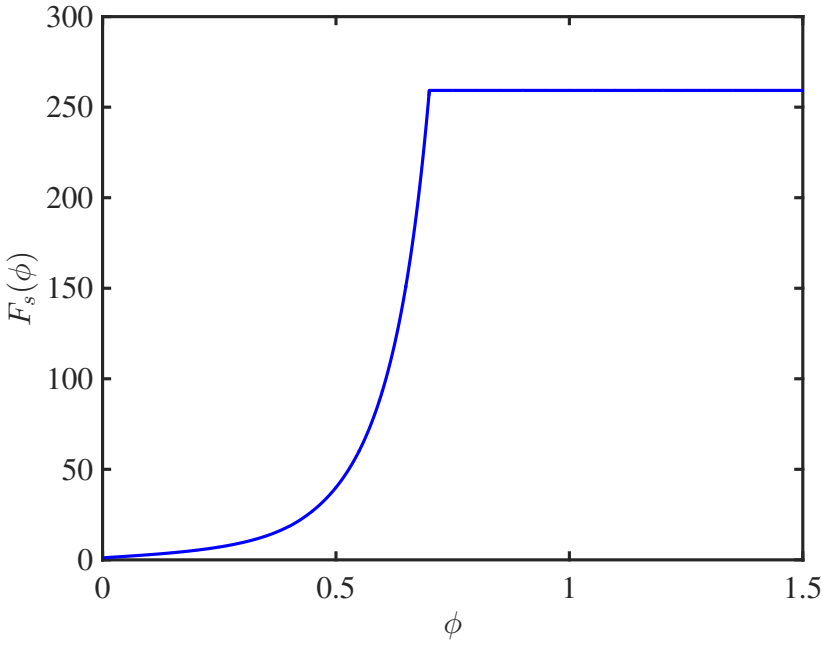

Figure 5.1: Segment drag coefficient $F_s(\phi)$ versus segment volume fraction ϕ.

.

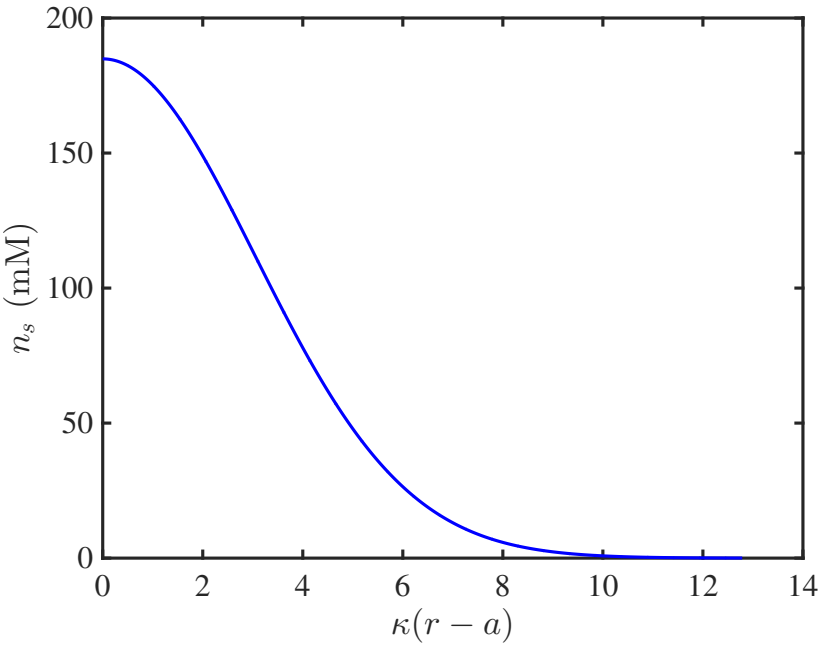

Figure 5.2: Radial distribution of segment density n_s for CM-5kPEG-Au NPs ($a =$ 2.7 nm) with layer thickness $\delta_1 = 4.14$ nm. Number of segment in a chain $N_s = 1$, segment friction radius $a_s = 1.7$ nm.

.

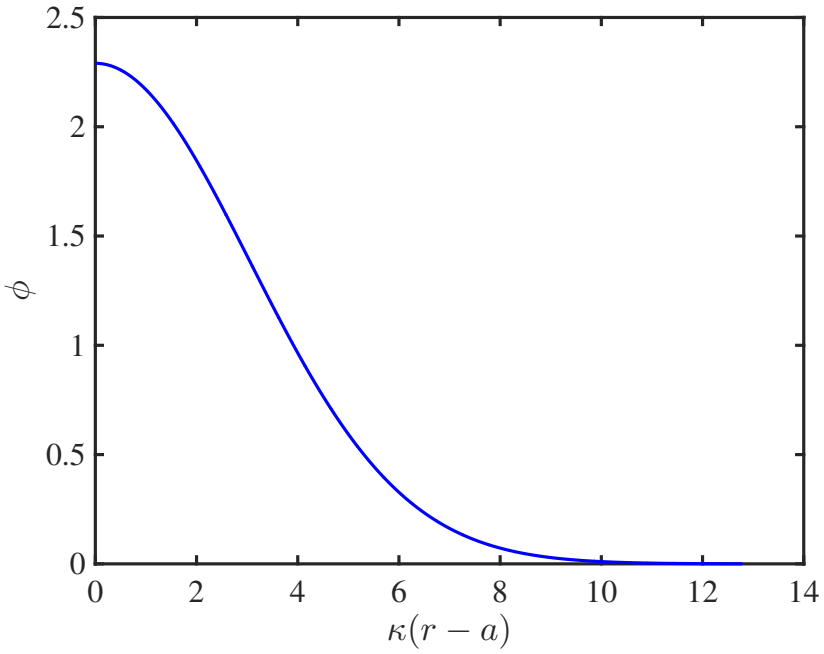

Figure 5.3: Radial distribution of segment volume fraction ϕ for CM-5kPEG-Au NPs ($a = 2.7$ nm) with layer thickness $\delta_1 = 4.14$ nm. Number of segment in a chain $N_s = 1$, segment friction radius $a_s = 1.7$ nm.

.

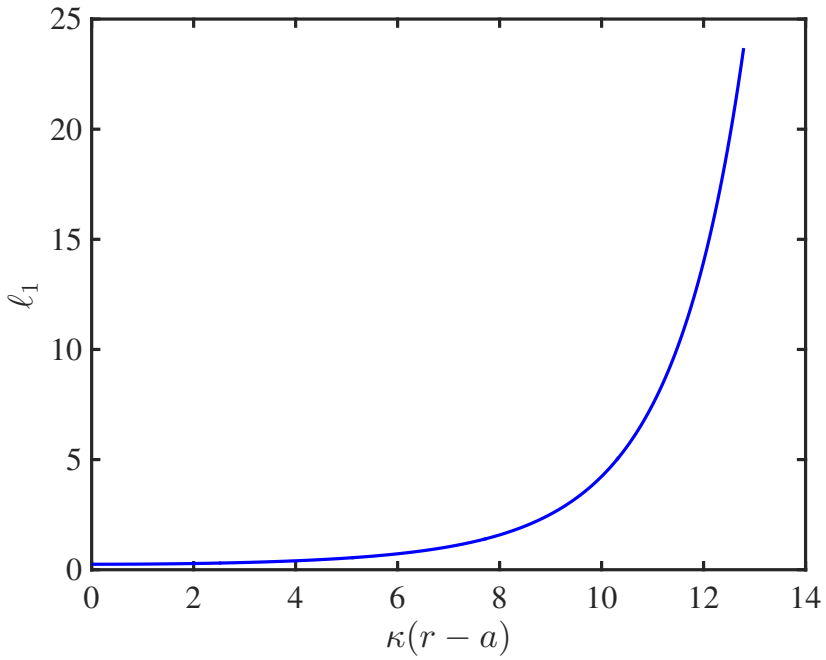

Figure 5.4: Radial distribution of Brinkman screening length ℓ_2 for CM-5kPEG-Au NPs ($a = 2.7$ nm) with layer thickness $\delta_1 = 4.14$ nm. Number of segments in a chain $N_s = 1$, segment friction radius $a_s = 1.7$ nm.

.

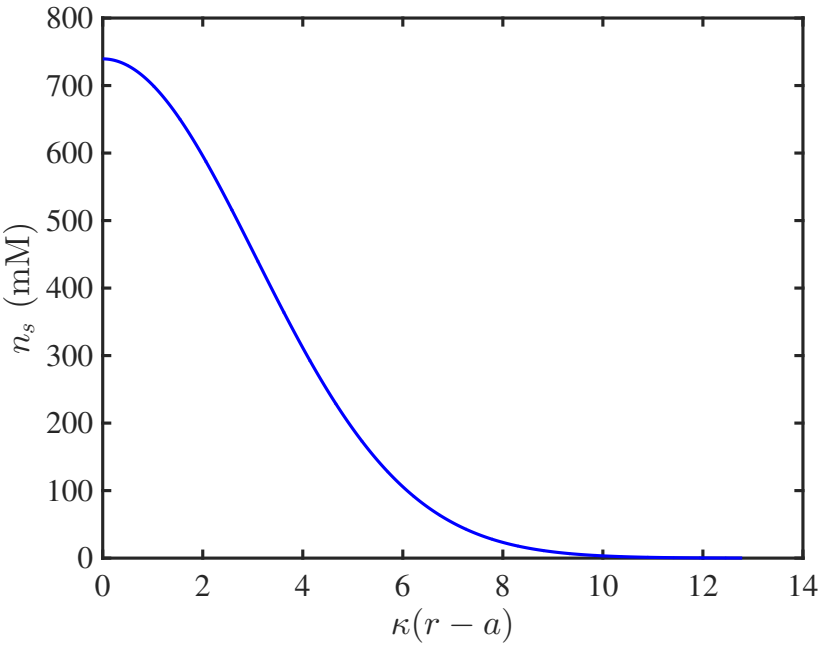

Figure 5.5: Radial distribution of segment density n_s for CM-5kPEG-Au NPs ($a = 2.7$ nm) with layer thickness $\delta_1 = 4.14$ nm. Number of segments in a chain $N_s = 4$, segment friction radius $a_s = 0.7$ nm.

.

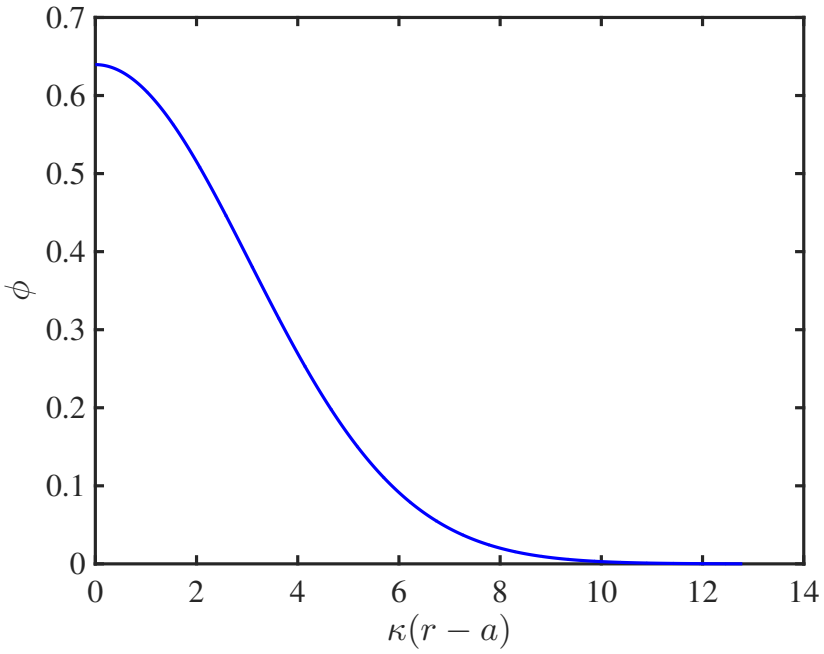

Figure 5.6: Radial distribution of segment volume fraction ϕ for CM-5kPEG-Au NPs ($a = 2.7$ nm) with layer thickness $\delta_1 = 4.14$ nm. Number of segments in a chain $N_s = 4$, segment friction radius $a_s = 0.7$ nm.

.

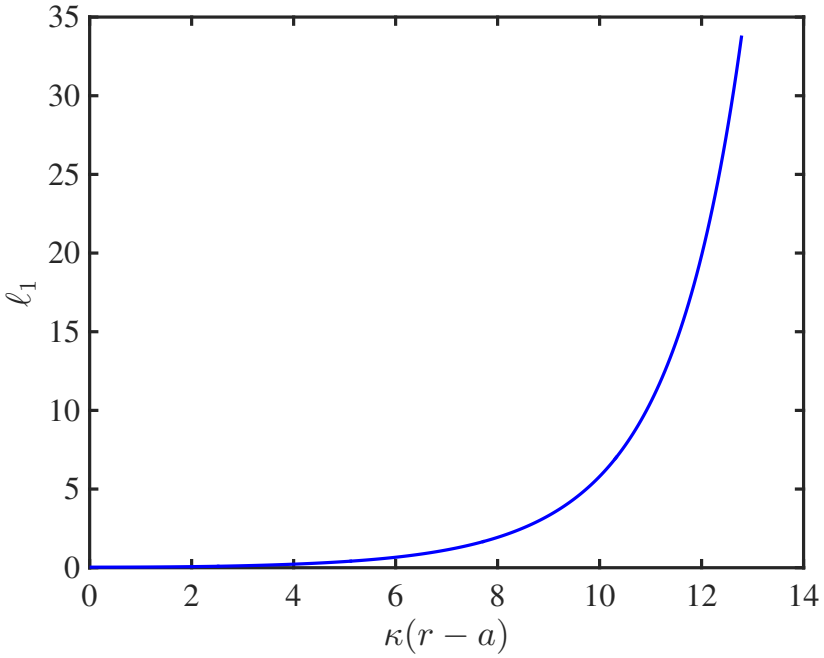

Figure 5.7: Radial distribution of Brinkman screening length ℓ_2 for CM-5kPEG-Au NPs ($a = 2.7$ nm) with layer thickness $\delta_1 = 4.14$ nm. Number of segments in a chain $N_s = 4$, segment friction radius $a_s = 0.7$ nm.

.

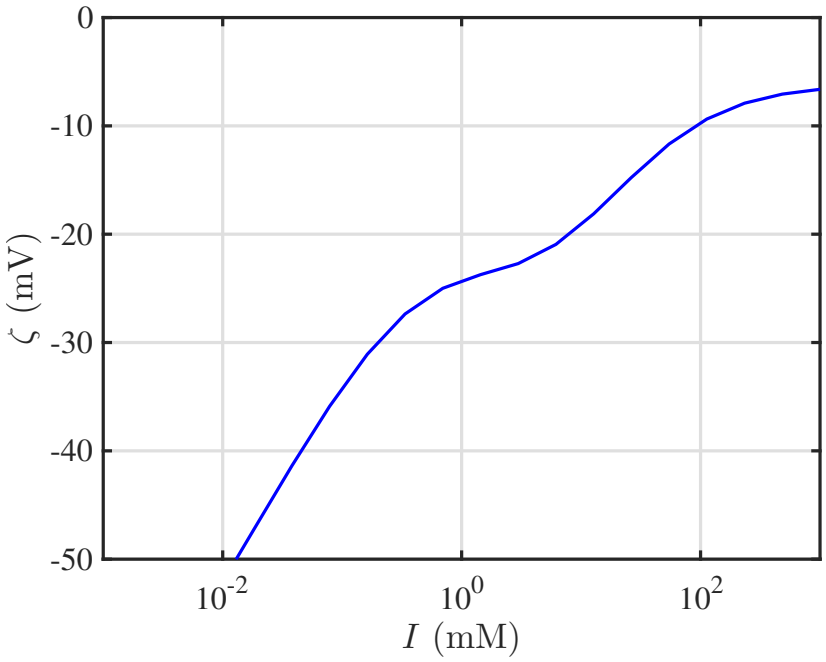

Figure 5.8: Calculation of free-solution electrophoretic mobilities for CM-5kPEG-Au NPs ($a = 2.7$ nm) with $N_s = 83$, $a_s = 0.07$ nm. Electrophoretic mobility reported as a Smoluchowski ζ potential (mV) versus ionic strength I (mM). The line passes through the experimental data shown in Hill et al. (2015).

.

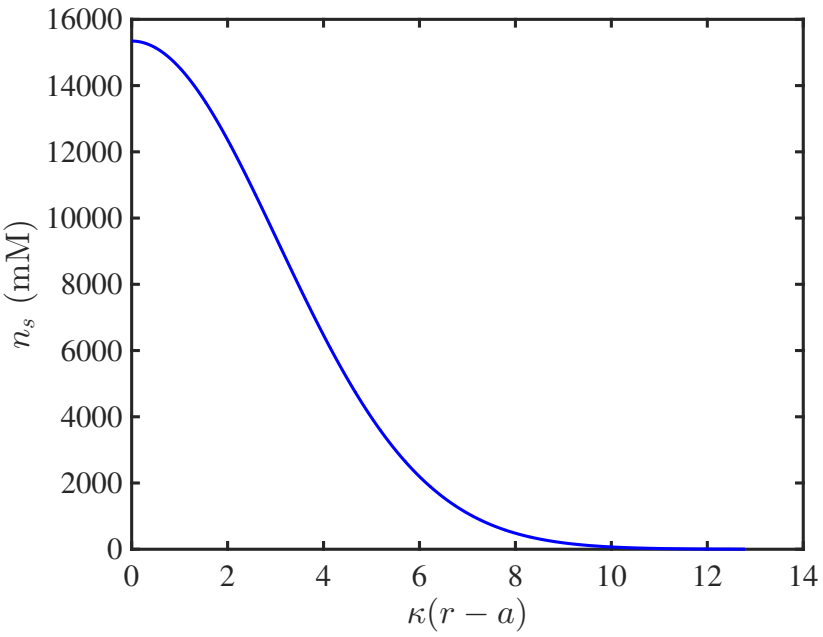

Figure 5.9: Radial distribution of segment density n_s for CM-5kPEG-Au NPs ($a = 2.7$ nm) with layer thickness $\delta_1 = 4.14$ nm. Number of segments in a chain $N_s = 83$, segment friction radius $a_s = 0.07$ nm.

.

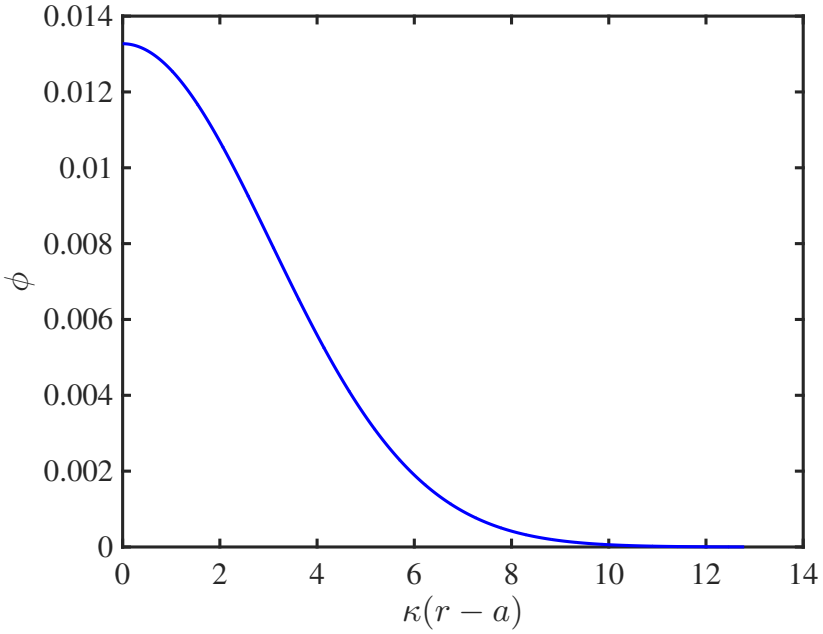

Figure 5.10: Radial distribution of segment volume fraction ϕ for CM-5kPEG-Au NPs ($a = 2.7$ nm) with layer thickness $\delta_1 = 4.14$ nm. Number of segments in a chain $N_s = 83$, segment friction radius $a_s = 0.07$ nm.

.

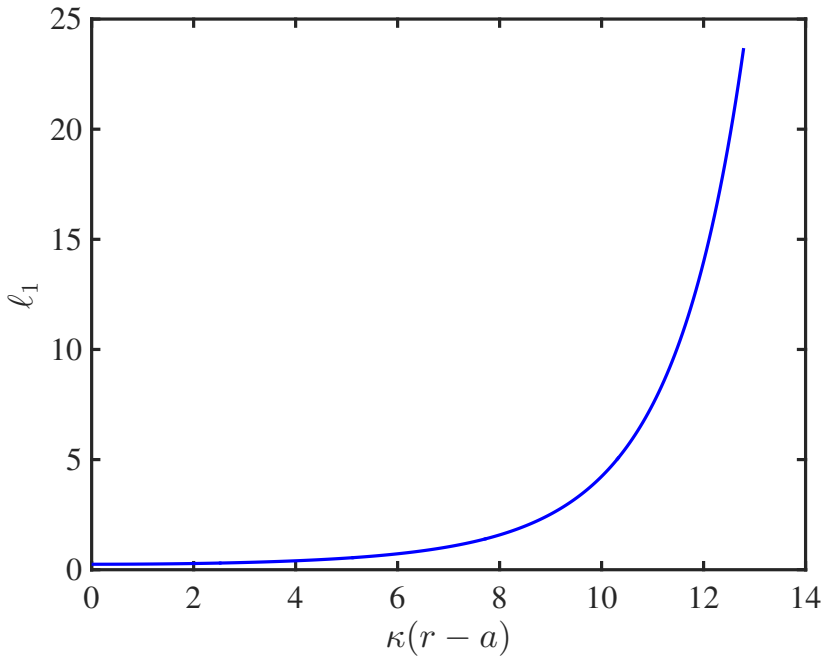

Figure 5.11: Radial distribution of Brinkman screening length ℓ_2 for CM-5kPEG-Au NPs ($a = 2.7$ nm) with layer thickness $\delta_1 = 4.14$ nm. Number of segments in a chain $N_s = 83$, segment friction radius $a_s = 0.07$ nm.

.